Copy 220
RM L56D30

RESEARCH MEMORANDUM

FREE-FLIGHT INVESTIGATION OF EFFECTS OF SIMULATED SONIC TURBOJET EXHAUST ON THE DRAG OF TWIN-JET BOATTAIL BODIES AT TRANSONIC SPEEDS

By Abraham Leiss

Langley Aeronautical Laboratory
Langley Field, Va.

NATIONAL ADVISORY COMMITTEE
FOR AERONAUTICS

WASHINGTON
July 20, 1956

NATIONAL ADVISORY COMMITTEE FOR AERONAUTICS

RESEARCH MEMORANDUM

FREE-FLIGHT INVESTIGATION OF EFFECTS OF SIMULATED SONIC TURBOJET EXHAUST ON THE DRAG OF TWIN-JET BOATTAIL BODIES AT TRANSONIC SPEEDS

By Abraham Leiss

SUMMARY

A flight investigation was made to determine the effect of a propulsive jet on the zero-lift drag characteristics of two twin-exit boattailed bodies at transonic speeds. The two models which had ratios of jet area to base area of 0.394 and 0.590 covered a Mach number range of 0.8 to 1.15 and Reynolds number range, based on body length, from 40×10^6 to 65×10^6. The jet exit static-pressure ratio varied from 3.45 to 3.95 and from 2.7 to 3.1 for models 1 and 2, respectively.

A slight reduction in drag coefficients from power-off values was obtained during power-on flight for both models. This drag reduction was caused mainly by the positive increments in base pressure coefficients observed between power-on and power-off flight conditions.

INTRODUCTION

Investigations of the effect of a propulsive jet on the drag of boattail bodies of revolution have shown that in many cases appreciable reductions in drag coefficients have been obtained with the jet operating as compared with jet-off conditions (refs. 1, 2, and 3). Since many large aircraft are using two engines in a single nacelle, it was proposed to investigate the effect of the jet on the drag of bodies which would have twin exhausts to see if the drag reduction with power on would be as favorable as those for single-engine installation. One other research investigation of twin exits is reference 4 which was made at a Mach number of 1.91. Therefore, as part of an investigation of the effect of sonic turbojet exhausts on body drag and base-pressure coefficients, the Langley Pilotless Aircraft Research Division made flight tests of two twin-jet bodies at transonic speeds with different jet exhaust sizes.

The two research models used solid-fuel rocket motors (designed according to ref. 5) to simulate turbojet exhausts and were flight tested at the Langley Pilotless Aircraft Research Station, at Wallops Island, Va.

The Mach number range was 0.8 to 1.15, and the Reynolds number range (based on body length) was 40×10^6 to 65×10^6.

SYMBOLS

A_b total base area, sq ft

A_e jet-exit area, sq ft

a_l longitudinal acceleration, ft/sec^2

C_D total drag coefficient $\left(\text{for power off, } C_D = \frac{D}{q_\infty S}\text{; for power on, } C_D = \frac{T - \frac{W}{g}a_l}{q_\infty S}\right)$

$C_{D,b}$ total base drag coefficient, $-C_{p,b}\frac{A_b}{S}$

$c_{p,b}$ local base pressure coefficient $\frac{p - p_\infty}{q_\infty/144}$

$C_{p,b}$ average base pressure coefficient

D drag force, lb

D' equivalent diameter used for fineness ratio, $\sqrt{\frac{4S}{\pi}}$

D_e diameter of each jet exit, in.

D_T diameter of throat of nozzle, in.

g acceleration due to gravity, ft/sec^2

l body length, in.

L propellant length, in.

M free-stream Mach number

M_e jet-exit Mach number

p static pressure, lb/sq in. abs

p_e jet-exit static pressure, lb/sq in. abs

p_∞ free-stream static pressure, lb/sq in. abs

q_∞ free-stream dynamic pressure, $144\gamma p_\infty M^2/2$, lb/sq ft

R Reynolds number, based on fuselage length (106 in.)

s distance between jet exits along base center line, in.

S maximum fuselage cross-sectional area, sq ft

T thrust, $2A_e\left[p_e\left(\gamma M_e^2 + 1\right) - p_\infty\right]$, lb

W weight, lb

γ ratio of specific heats

MODELS AND APPARATUS

Model Description

Sketches and photographs of the models are shown in figures 1 to 5. Both models were designed with a parabolic nose, a 6.32-inch transition section from 6.612 inches diameter to a 10.313-inch by 5.39-inch oval, a straight oval section, and a 7.5° boattail about the exhausts. A smooth notched fairing reaching a maximum boattail angle of 10.3° at the center of the oval was made between the jet center lines for the purpose of reducing the base area. The total length of each model was 106 inches, with an equivalent fineness ratio (l/D') of 13.378. The ratios of jet area to base area were 0.590 and 0.394 for models 1 and 2, respectively.

Four 45° delta fins, with a flat-plate airfoil beveled 10° at the leading and trailing edges, were mounted on the body with the trailing edge 7 inches ahead of the base of the model. As shown in figure 1, the fins had an aspect ratio of 2 per panel and the exposed area of each panel was 0.50 square foot.

Illustrated in figure 3 is a cross section of the turbojet simulators that were installed in the models. All parts of the simulator were identical in each model except for the throat diameters, and the exit diameters, which are tabulated in figure 3. Cordite Su/k propellant grains (ref. 5) were used in the jet simulators. The pair of propellant grains for models 1 and 2, weighed 14.9 pounds and 10.7 pounds, respectively. The Su/k propellant grains were placed inside modified 3.25-inch rocket

cases that were fitted with a common headcap. The igniter was placed inside this dual headcap.

Instrumentation

The models were each instrumented with a 10-channel telemeter, which was used to transmit measurements of free-stream total pressure, longitudinal acceleration, combustion-chamber pressure, and seven individual base pressures. The midsection of the base of model 1 was instrumented with seven orifices. Model 2 had six orifices in the midsection of the base and one on the base annulus. The model base and location of the base-pressure orifices used for flight measurement are shown in figure 5. The location of the free-stream total-pressure tube is shown in figure 1. The static pressure was measured in the rear of the rocket combustion chamber as shown in figure 3.

Velocity and Mach number of the test models were obtained by the use of continuous-wave Doppler radar and by the integration of the data from the longitudinal accelerometer. The trajectories of the models were obtained by NACA modified SCR-584 tracking radar. Atmospheric data and wind characteristics for each flight were obtained by means of a balloon carrying a radiosonde sent aloft at the time of each flight.

Booster

Both models were boosted with 65-inch HVAR rocket motors. A photograph of the model and booster on the launcher is shown in figure 4.

TESTS AND ANALYSIS

Flight Tests

After being accelerated to a Mach number of approximately 1.0, the models separated from the boosters and zero-lift power-off data were obtained during the coasting flight. At approximately a Mach number of 0.85, the sustainer motor ignited and power-on data were recorded as the models accelerated to the maximum Mach number. Power-off data were also recorded as the model decelerated after the sustainer burned out.

Ground Test

A typical $3\frac{1}{4}$-inch modified rocket case loaded with a cordite Su/k sustainer, identical to those described previously in the section entitled,

"Model Description" was fired on a thrust stand. Combustion-chamber pressure and thrust were measured with respect to time for this static test. The jet-exit static pressure p_e was computed from the following equation:

$$p_e = \frac{T + p_\infty A_e}{A_e(\gamma M_e^2 + 1)}$$

A calibration curve of jet-exit static-pressure variation with combustion-chamber pressure was developed. The combustion-chamber pressure was measured in flight to determine jet-exit static pressure from the calibration curve. From the jet-exit static pressure, the thrust at altitude was determined and used to determine power-on drag. This is expressed in the following equation:

$$C_D = \frac{T - \frac{Wa_l}{g}}{q_\infty S}$$

ACCURACY

The description of the accuracy limits for this type testing is presented in reference 1. Values at three representative Mach numbers are presented in the following table:

Maximum Possible Errors				
M	ΔM	$C_{p,b}$	$C_{D,off}$	$C_{D,on}$
0.85	±0.010	±0.0044	±0.0017	±0.0357
1.02	±.005	±.0030	±.0080	±.0232
1.15	±.005	±.0025	±.0147	±.0187

It should be emphasized that general consideration of the results indicates that the degree of accuracy for the present data is considerably better than that expressed by the tabulated results which reflect random errors occurring over a comparatively large number of tests.

[redacted]

RESULTS AND DISCUSSION

The variation of Reynolds number based on body length with free-stream Mach number for the tests is shown in figure 6. At a typical Mach number of 1.00, note that the Reynolds number varies from 60×10^6 for the power-off first coast to 58×10^6 for the power-on flight and to 52×10^6 for the power-off second coast. The decrease in 1st and 2nd coast power-off values, shown in figure 6, is because of the difference in altitude.

The variation of jet static-pressure ratio with free-stream Mach number is shown in figure 7.

Drag

The variation of power-on and power-off total drag coefficients with Mach number for models 1 and 2 is presented in figure 8. The power-on drag coefficients are lower than the power-off drag coefficients over the Mach number range for which power-on data are presented. However, model 1 has appreciably lower power-on drag coefficient than model 2 from Mach number 0.95 to 1.05. In reference 1, for conical boattail bodies of revolution, no differences of this magnitude in total drag coefficients were found between models with different ratios of jet area to base area. However, from figure 7, it may be seen that a difference in jet-exit static pressure exists. The jet static-pressure ratios should have been similar, but model 1 had a lower value of p_e/p_∞ than expected. It was shown in reference 3 that differences in jet static-pressure ratio can produce large differences in power-on drag coefficients at transonic speeds. Thus, it is felt that the major difference between the power-on drag coefficients of models 1 and 2 was caused by the difference in jet-exit static-pressure ratio and that the differences due to A_e/A_b (ratio of jet area to base area) and s/D_e (jet spacing ratio) were of smaller magnitude.

Reference 4 shows that a change in spacing ratio s/D_e from 1.4 to 1.7 has little effect on base pressure coefficients at jet static-pressure ratios of 3 to 4. Models 1 and 2 had jet spacing ratios of 1.56 and 1.91, respectively. Therefore, large changes in base pressure coefficients cannot be attributed to the difference in jet spacing ratio for these two models. In reference 3, changing the ratio A_e/A_b from 0.844 to 0.706 had practically no effect on the base pressure coefficients. However, when the ratio A_e/A_b was changed to 0.563 a slight reduction in base pressure coefficients and a slight increase in total drag coefficients was obtained. Since models 1 and 2 had ratios of jet area to base area

of 0.590 and 0.394, any appreciable change in base pressure coefficients or total drag coefficients is probably not attributed to this change in A_e/A_b.

Because of the difference in jet static-pressure ratio the jet exhausts were different in nature. The larger exhaust stream of model 1 intersects with the free-stream flow over the body and boattail causing different effects than the flow over the boattail intersecting the smaller exhaust stream of model 2. The higher pressure ratio of model 1 caused the primary shock to hold a more forward position on the boattail than on model 2. A favorable power-on boattail drag resulted and is included in the favorable power-on total drag.

At Mach numbers greater than 1.05, the total drag coefficients of models 1 and 2 are nearly equal with model 1 having slightly lower drag coefficients.

Base Pressure Coefficients

Figure 9 shows the variation of power-on and power-off local base pressure coefficients with free-stream Mach number for the 14 orifices of models 1 and 2. The base pressure of all orifices increased from power-off to power-on flight conditions. Most of the base-pressure orifices of models 1 and 2 are located in different relative positions. However, orifices C of model 1 and J of model 2 are located at the center of the base and a direct comparison of base pressure coefficients can be made. Except at Mach number 0.95 where a very rapid change occurs in pressure coefficients, the curves of base-pressure coefficient are similar in shape. In general, similarly located orifices have similar variations in base pressure coefficient with Mach number although model 1 has slightly greater power-on base pressure coefficients than model 2. This shows a similar trend to reference 1 where the base pressure coefficients increased as the jet area ratio A_e/A_b increased. However, the difference in jet-exit static-pressure ratio, as described, was probably responsible for a major portion of the increase.

Figure 10 shows the power-on and power-off base-pressure-coefficient distribution along the horizontal center line of the base for various free-stream Mach numbers. Note the change from negative to positive pressures from power-off to power-on flight. Figure 11 shows the same pressure-coefficient distribution along a vertical line of the base. Note that the distribution is less uniform for power-on than power-off conditions.

The base of the models was geometrically divided into areas that were assigned to the individual orifices. Table 1 and the accompanying sketch show the percentage of base area computed for each orifice.

Figure 12 presents the variation of the integrated base pressure coefficients as they vary with free-stream Mach number for both models. The only large difference in these average base pressure coefficients is during supersonic power-on flight. This is primarily attributed to a smaller jet static-pressure ratio (p_e/p_∞) for model 2 as described. At a typical Mach number of 1.1, model 1 had only half as much increase from power-off to power-on pressure coefficient as did a single exit model having the same simulator as in reference 1. Also, model 2 had only one-third as much power-on pressure-coefficient increase as did a single-exit model having an identical simulator as in reference 1.

Base Drag

Figure 13 shows the variation of base drag coefficients with free-stream Mach number. The base drag was computed from the integrated base pressures of figure 11 $\left(C_{D,b} = -C_{p,b}\frac{A_b}{S}\right)$. The base-drag differentials are only prominent above a Mach number of about 0.95.

As shown in figure 14, the difference in power-on and power-off base drag accounts for most of the difference in power-on and power-off total drag of model 2 for Mach numbers below 1.05. The change in base drag fails substantially to account for this difference in model 1 at the same speeds. As the Mach number increases to 1.15 the base drag change fails to account for the increasing reduction in total power-on drag coefficients in both cases. Since the total base drag is about the same for the two models, a favorable fin and boattail effect is indicated with the effect being particularly powerful for model 1 at Mach numbers less than 1.05.

The fact that this favorable boattail effect is approximately the same for both models at the upper test limit, is considered coincidental and is not necessarily indicative of what might happen with different combinations of base area, jet spacing ratio, and static-pressure ratios.

SUMMARY OF RESULTS

Transonic free-flight tests at zero lift have been made on two twin jet-exit models to find the effect of jet operation on zero-lift drag coefficients. The tests covered a Mach number range from 0.8 to 1.15, a jet static-pressure ratio range from 2.7 to 3.9, and a Reynolds number range from 40×10^6 to 65×10^6 based on body length. The results are as follows:

1. Power-on drag coefficients were lower than power-off drag coefficients for the Mach number range tested.

2. Positive power-off to power-on base-pressure-coefficient increments were obtained for both models. For model 2, the base drag accounted for most of the incremental drag over most of the test Mach number range.

3. Measured differences in base pressure coefficients due to power effects were considerably less than for a single exit model having an identical simulator.

4. The model with the larger jet static-pressure ratio had a large decrease in transonic jet-on drag coefficients, probably due to favorable boattail drag.

Langley Aeronautical Laboratory,
National Advisory Committee for Aeronautics,
Langley Field, Va., April 11, 1956.

REFERENCES

1. Falanga, Ralph A.: A Free-Flight Investigation of the Effects of Simulated Sonic Turbojet Exhaust on the Drag of a Boattail Body With Various Jet Sizes From Mach Number 0.87 to 1.50. NACA RM L55F09a, 1955.

2. Falanga, Ralph A.: A Free-Flight Investigation of the Effects of a Sonic Jet on the Total-Drag and Base-Pressure Coefficients of a Boattail Body of Revolution From Mach Number 0.83 to 1.70. NACA RM L55L21, 1956.

3. Henry, Beverly Z., Jr., and Cahn, Maurice S.: Preliminary Results of an Investigation at Transonic Speeds to Determine the Effects of a Heated Propulsive Jet on the Drag Characteristics of a Related Series of Afterbodies. NACA RM L55A24a, 1955.

4. Salmi, Reino J., and Klann, John L.: Investigation of Boattail and Base Pressures of Twin-Jet Afterbodies at Mach Number 1.91. NACA RM E55C01, 1955.

5. De Moraes, Carlos A., Hagginbothom, William K., Jr., and Falanga, Ralph A.: Design and Evaluation of a Turbojet Exhaust Simulator, Utilizing a Solid-Propellant Rocket Motor, for Use in Free-Flight Aerodynamic Research Models. NACA RM L54I15, 1954.

TABLE 1

BASE AREA DISTRIBUTION FOR EACH ORIFICE

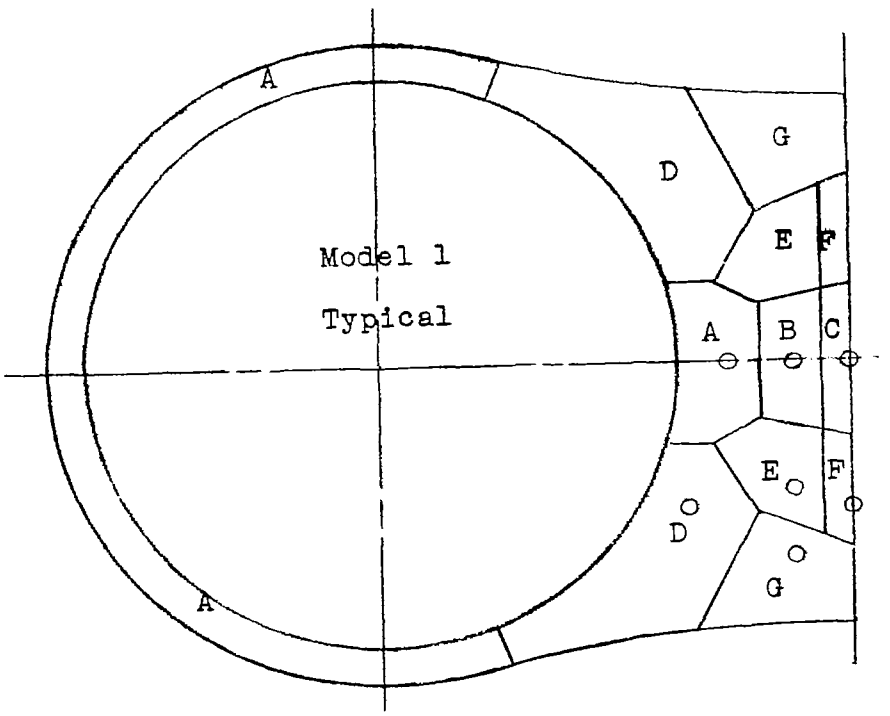

Model 1

A, percent	34.0
B, percent	4.7
C, percent	2.3
D, percent	31.4
E, percent	9.4
F, percent	3.6
G, percent	14.6

Model 2

H, percent	3.8
I, percent	3.3
J, percent	3.9
K, percent	11.8
L, percent	20.0
M, percent	16.2
N, percent	41.0

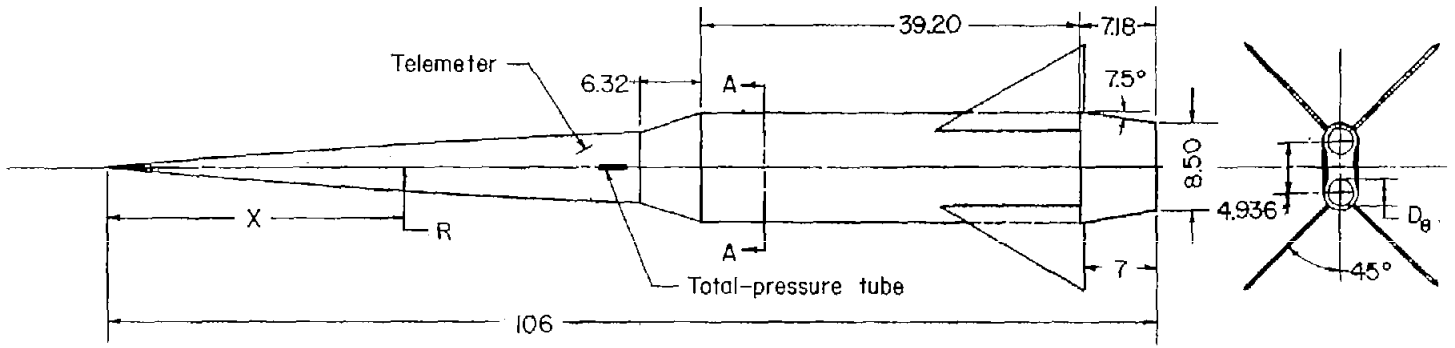

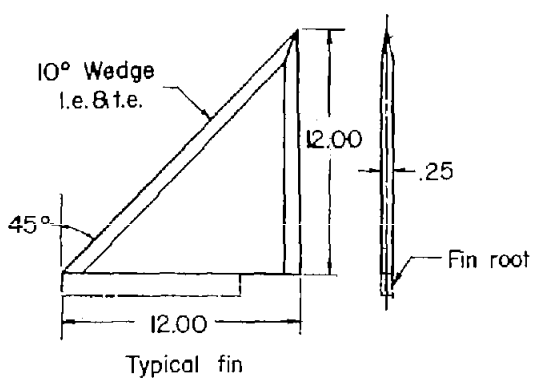

X, inches	R, inches
0	0
5.0	.482
10.0	.929
15.0	1.339
20.0	1.714
25.0	2.054
30.0	2.357
35.0	2.625
40.0	2.857
45.0	3.054
50.0	3.214
53.3	3.306

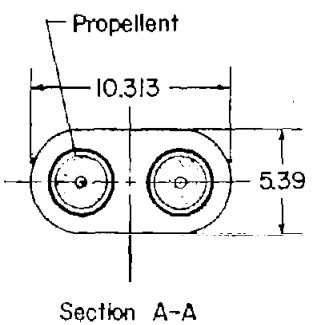

Model	D_e	A_e/A_b
1	3.163	.590
2	2.585	.394

Figure 1.- General arrangement of flight models. All dimensions are in inches.

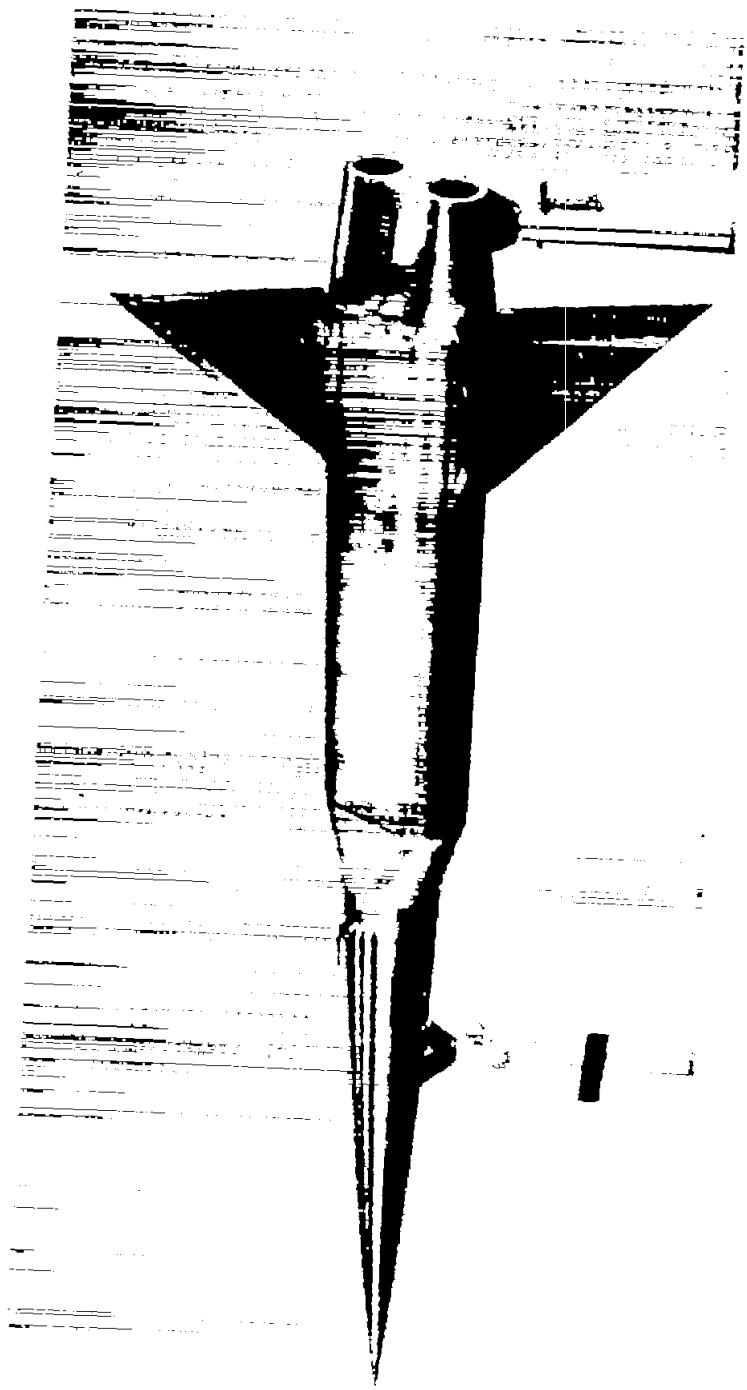

L-88610

Figure 2.- Photograph of flight model 2.

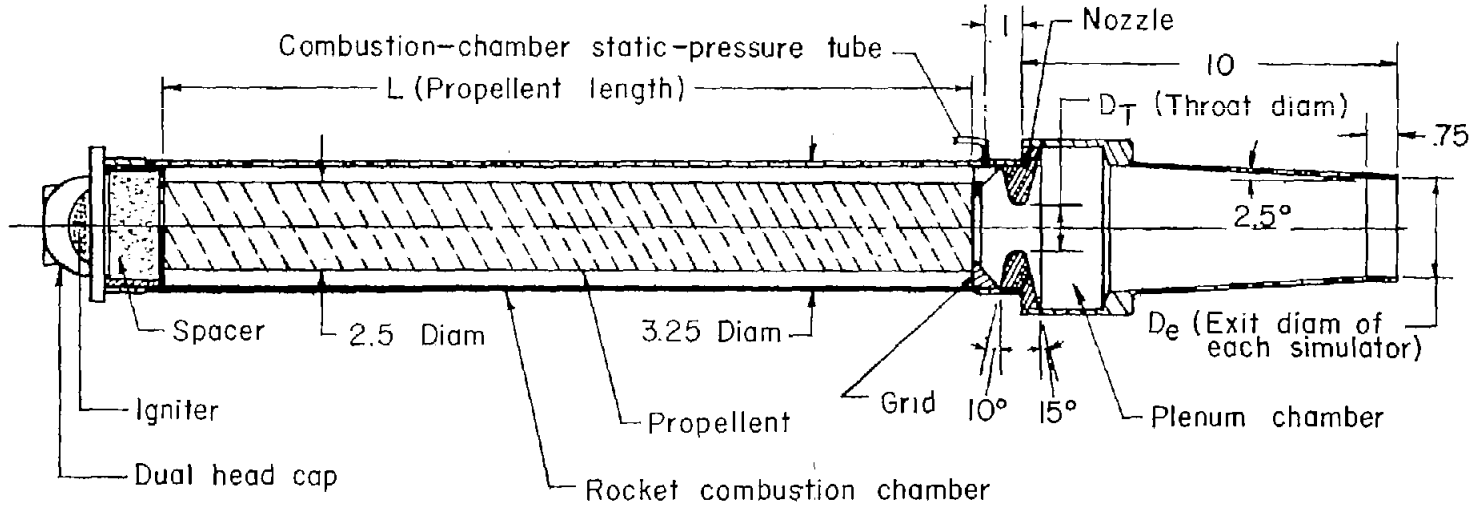

Model	D_e	D_T	L
1	3.163	1.336	29.7
2	2.585	1.158	21.4

Figure 3.- Cross section of a typical turbojet simulator. All dimensions are in inches.

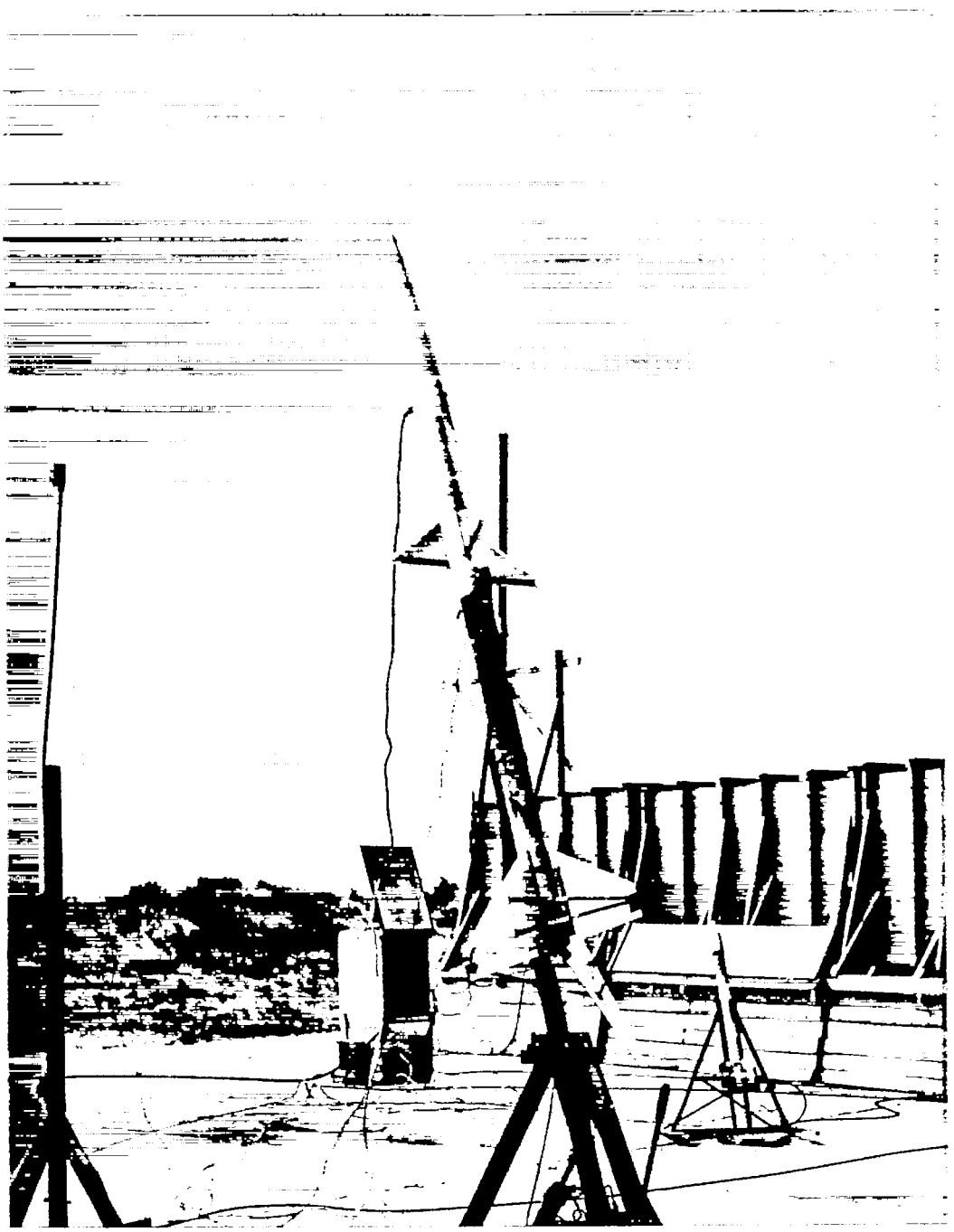

Figure 4.- Photograph of model 1 and booster on launcher. L-89148.1

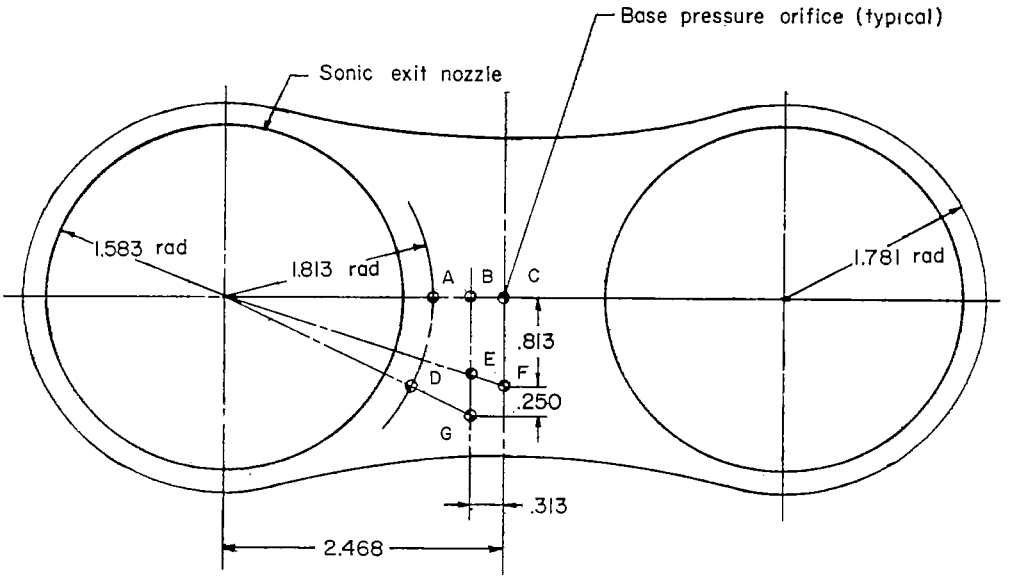

(a) Model 1.

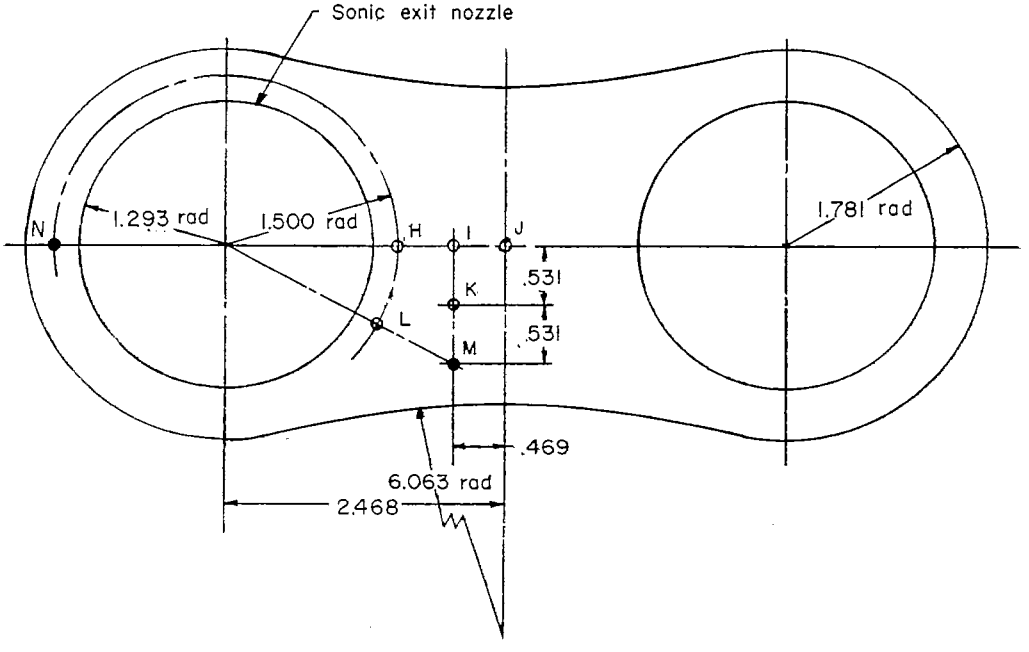

(b) Model 2.

Figure 5.- Sketch showing base and base-pressure orifice locations. All dimensions are in inches.

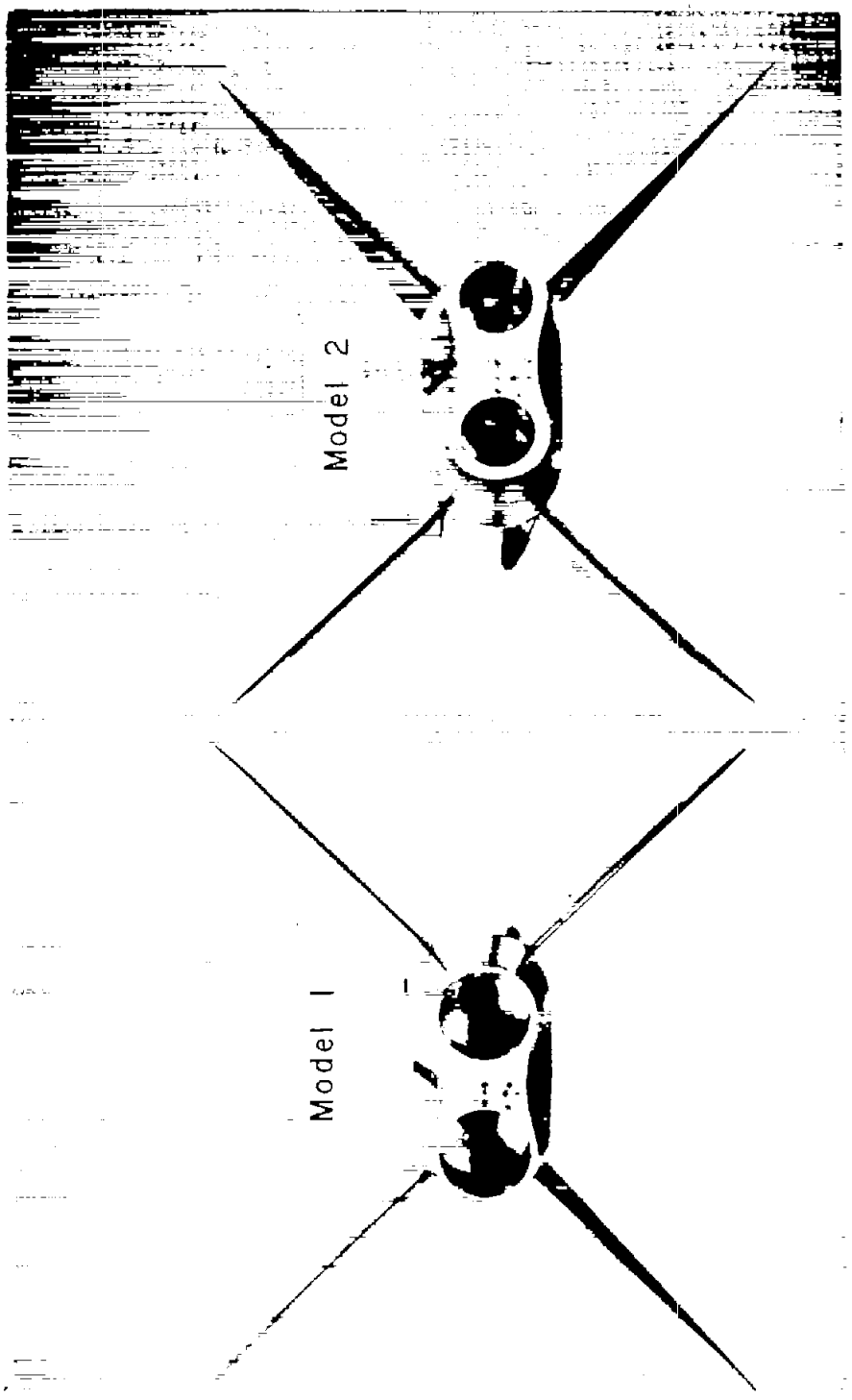

L-88612.1

(c) Photograph of bases.

Figure 5.- Concluded.

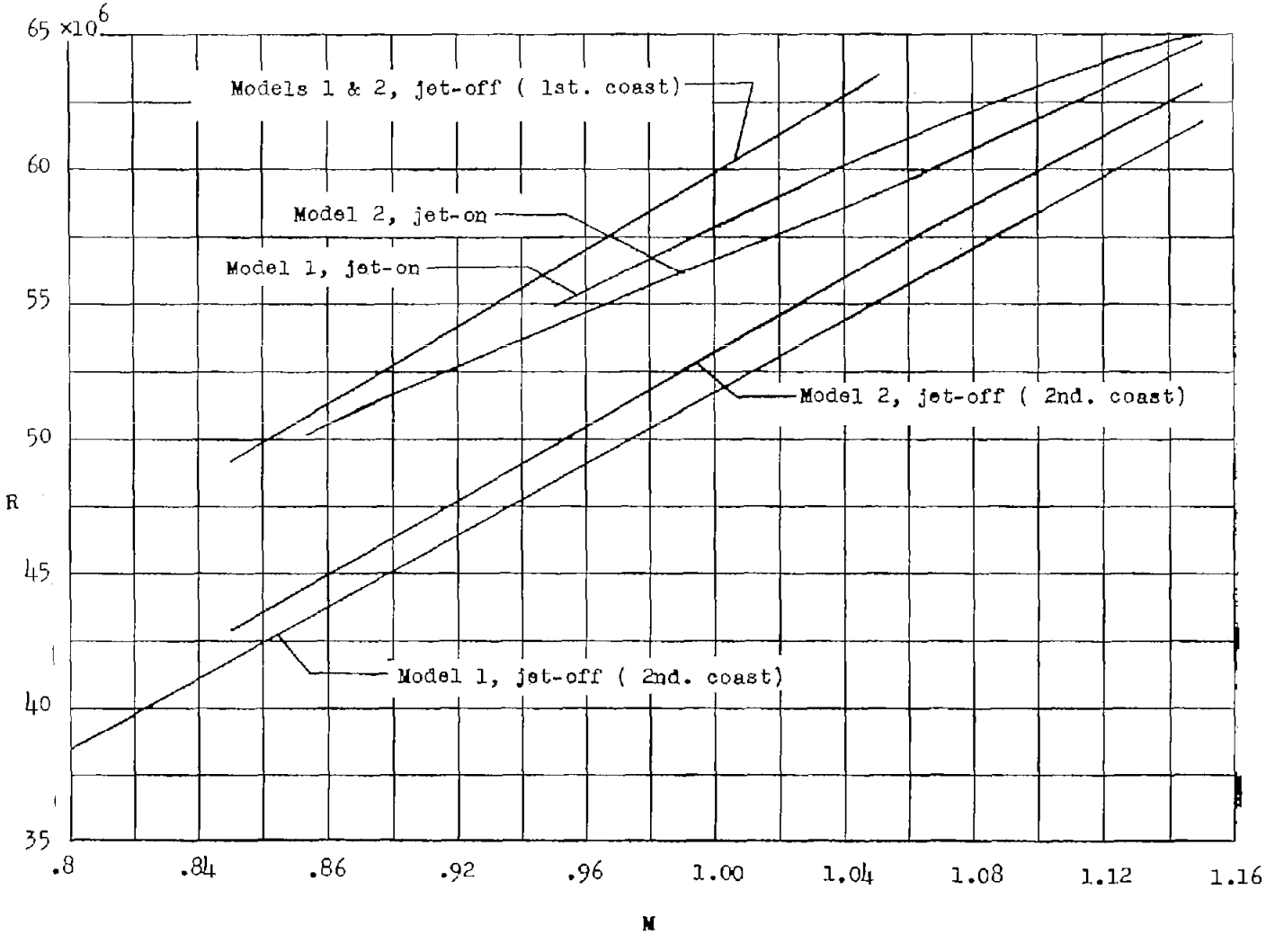

Figure 6.- Reynolds number (based on fuselage length, 106 in.) variation with free-stream Mach number.

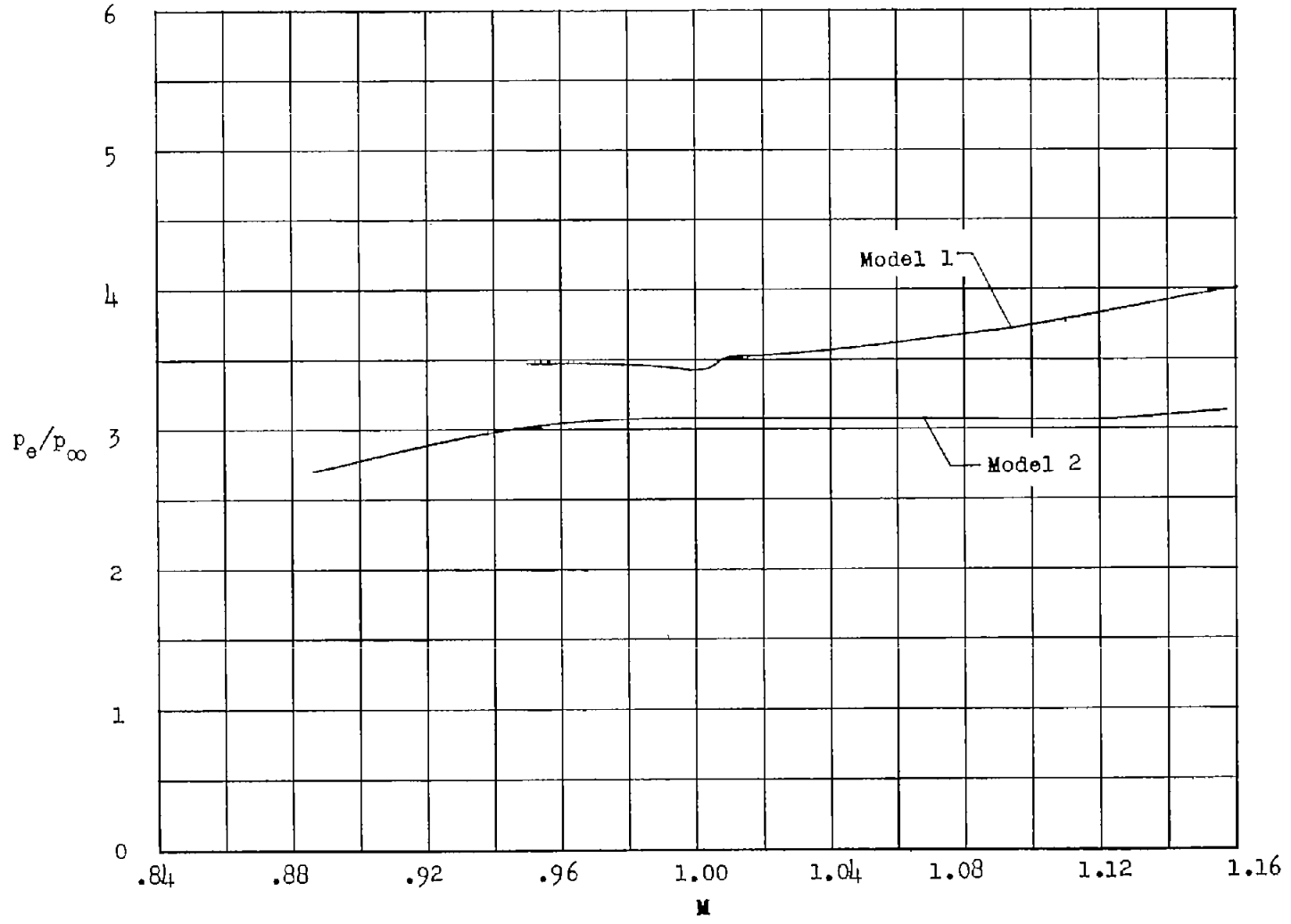

Figure 7.- Variation of jet static-pressure ratio with free-stream Mach number.

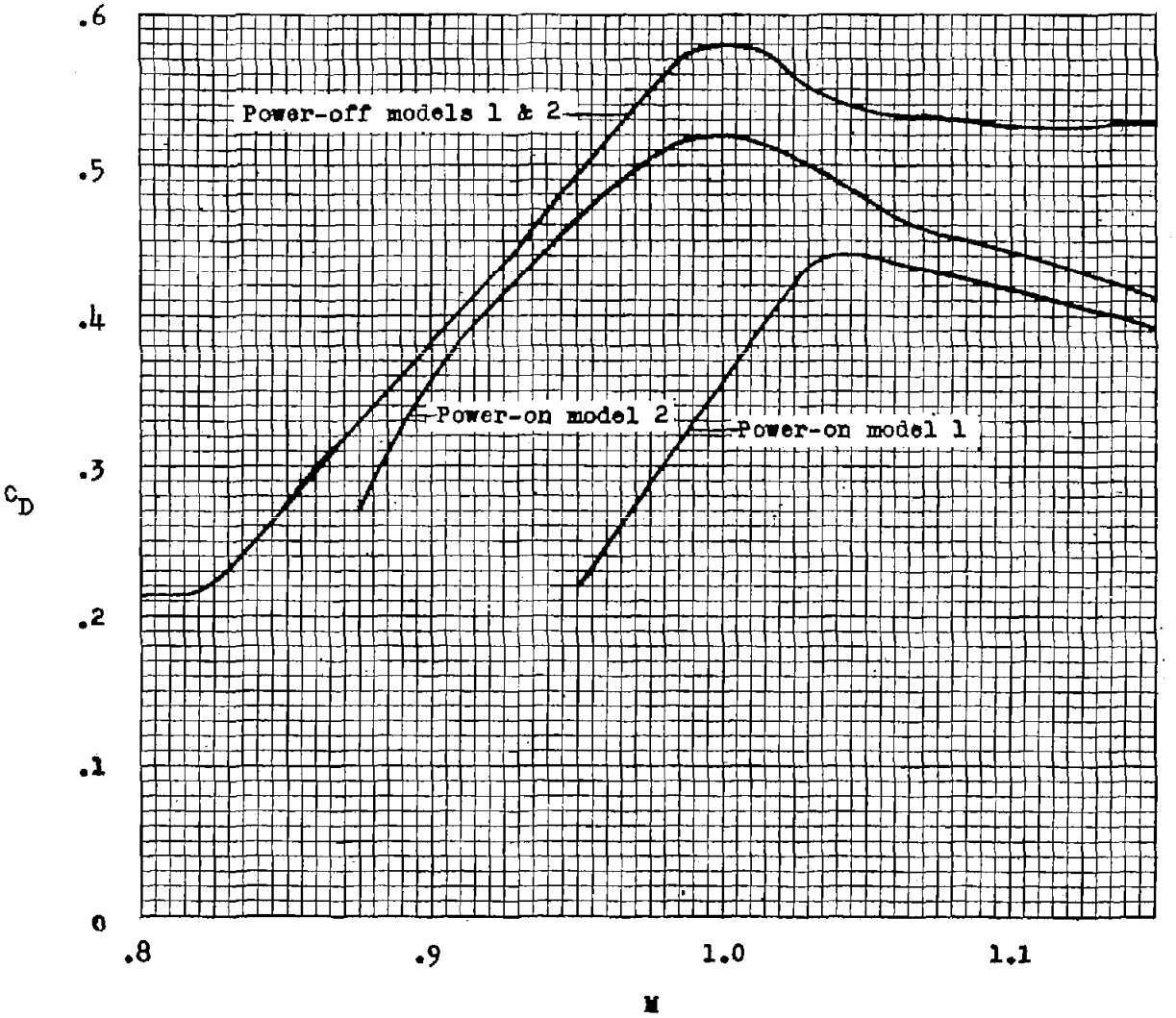

Figure 8.- Variation of power-on and power-off total drag coefficients with free-stream Mach number.

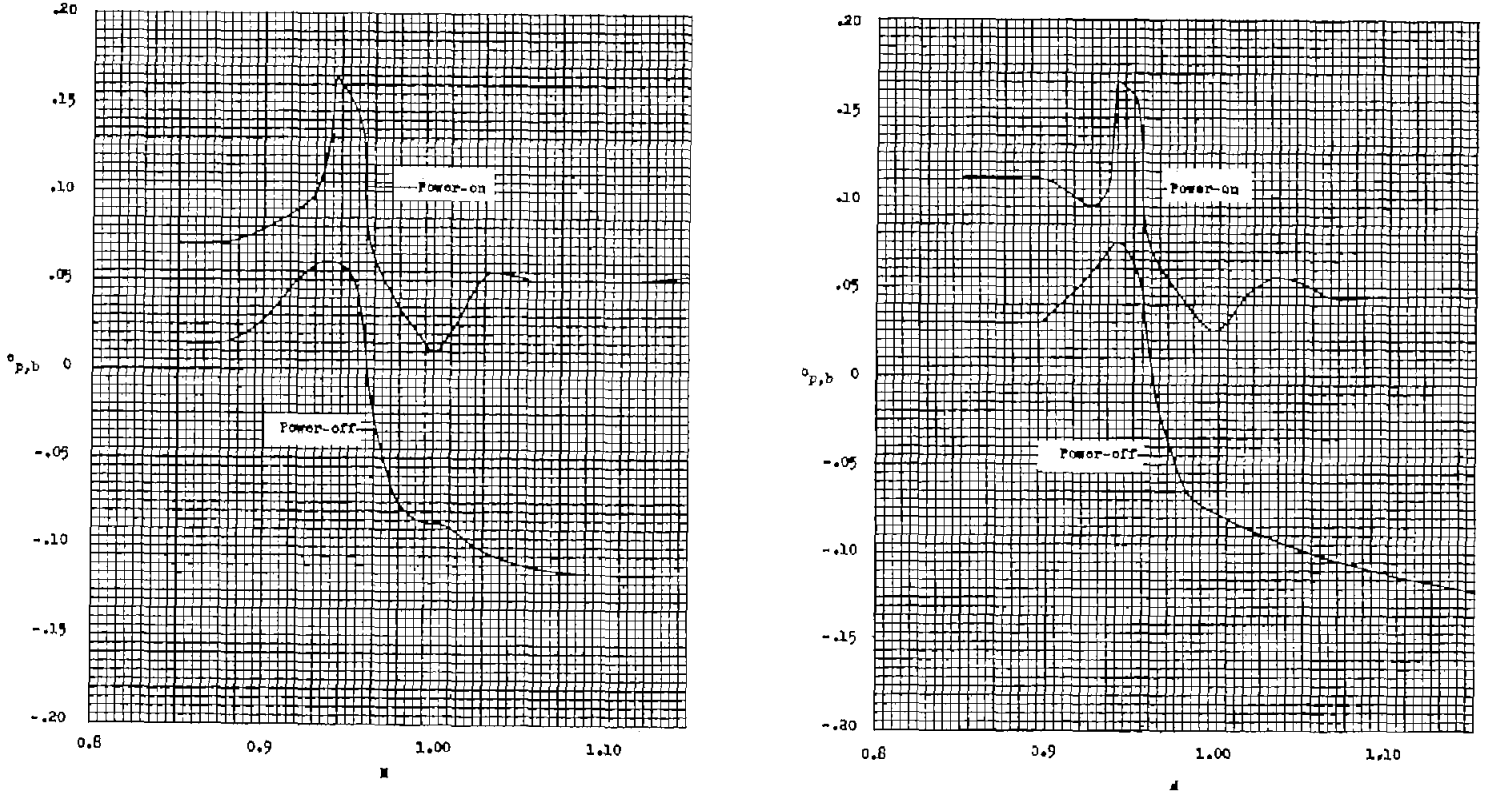

(a) Orifice A, model 1.

(b) Orifice B, model 1.

Figure 9.- Variation of base pressure coefficient with free-stream Mach number for each base-pressure orifice.

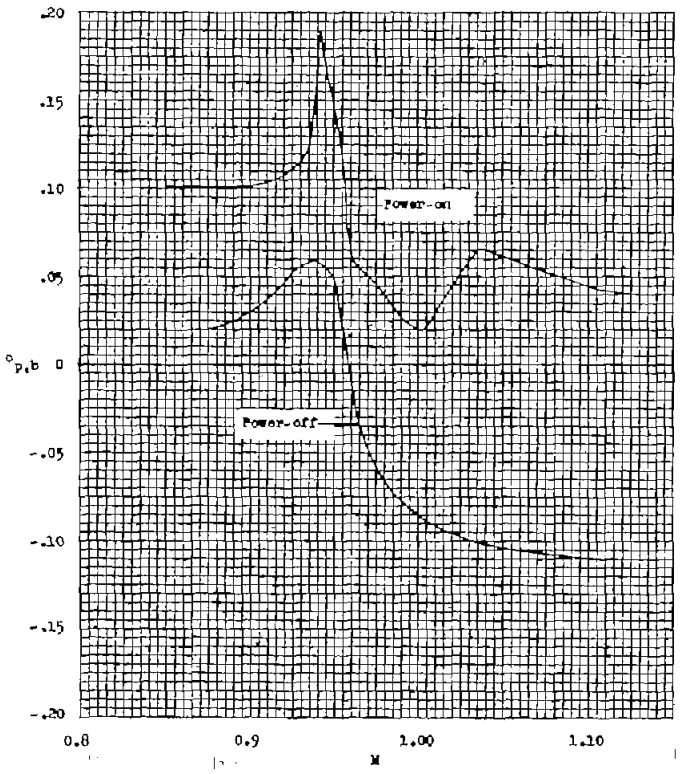

(c) Orifice C, model 1.

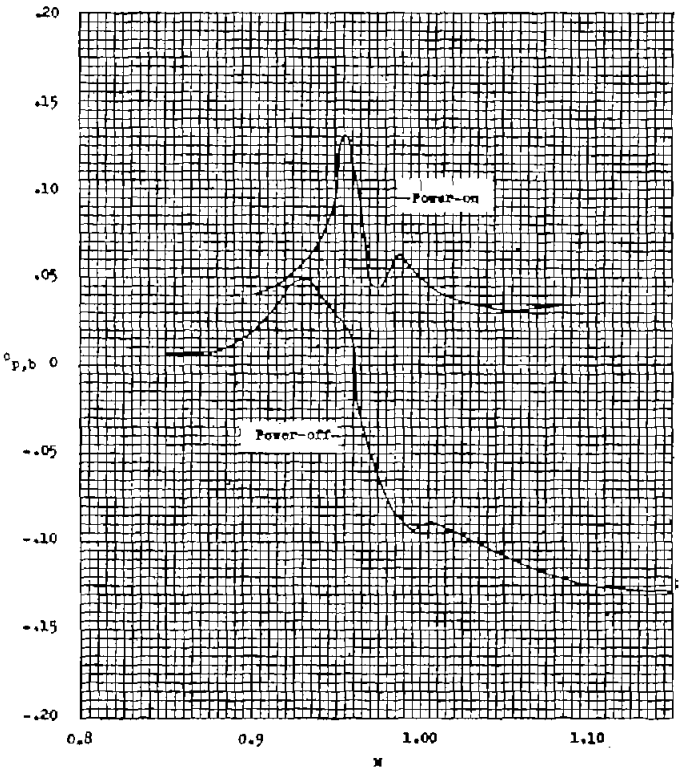

(d) Orifice D, model 1.

Figure 9.- Continued.

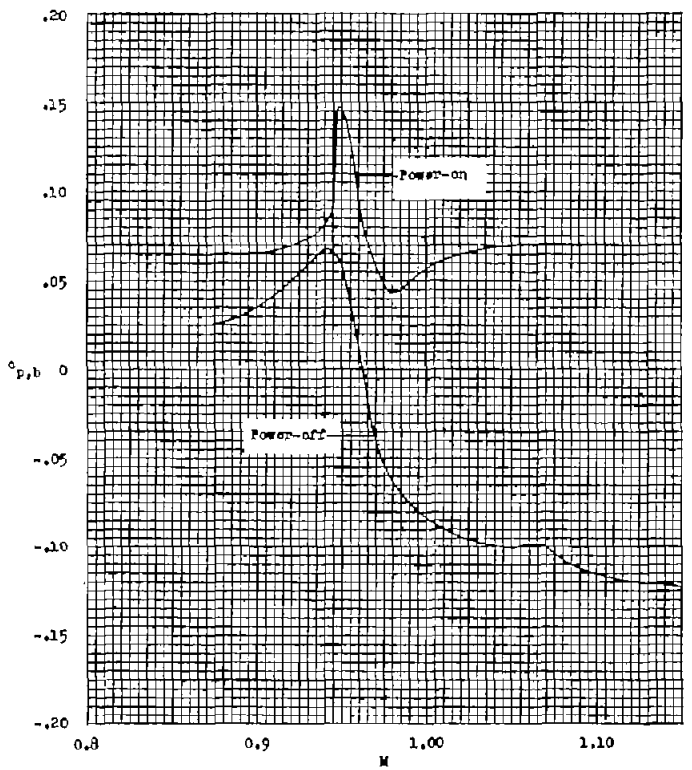

(e) Orifice E, model 1.

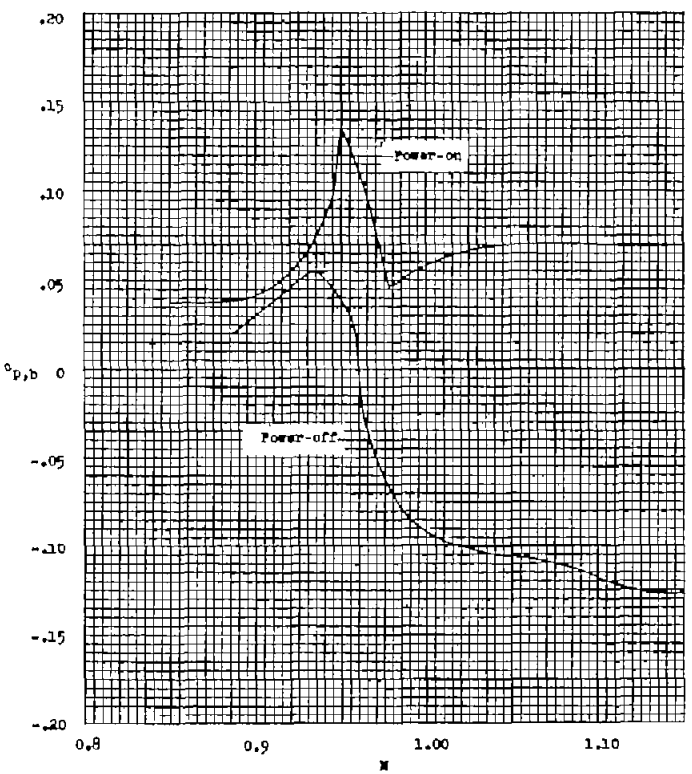

(f) Orifice F, model 1.

Figure 9.- Continued.

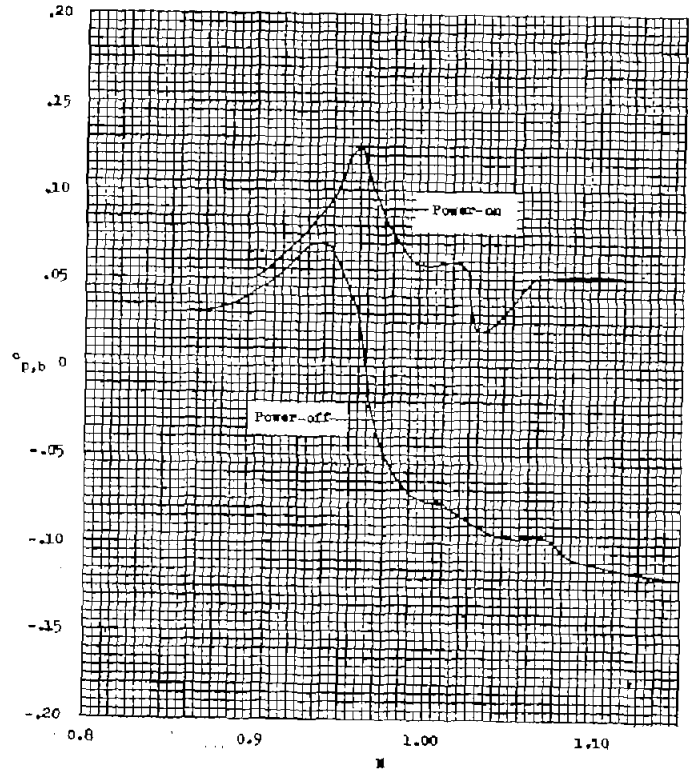

(g) Orifice G, model 1.

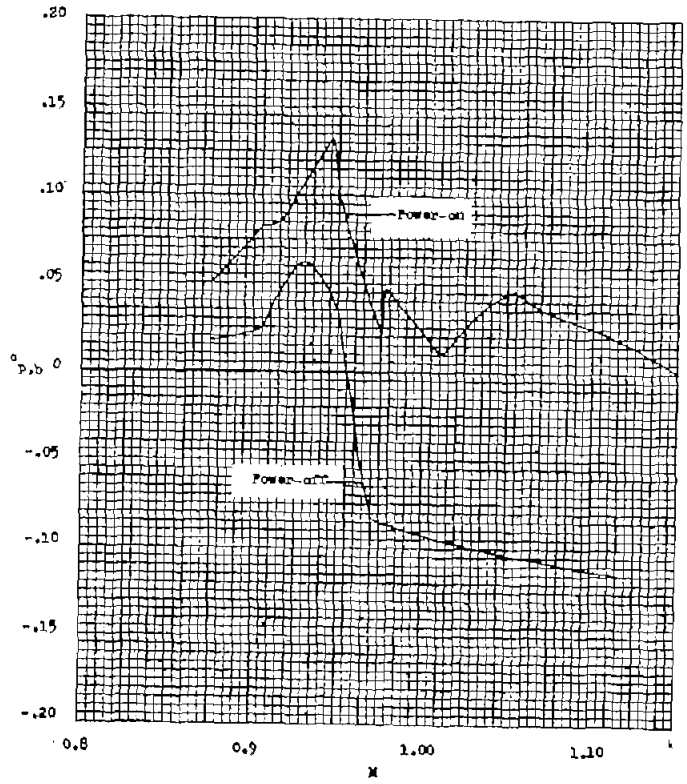

(h) Orifice H, model 2.

Figure 9.- Continued.

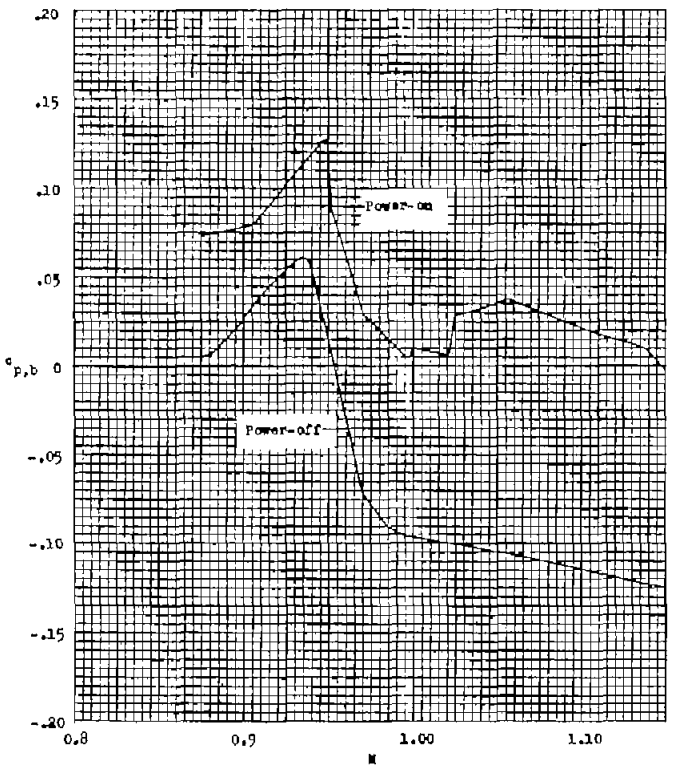

(i) Orifice I, model 2.

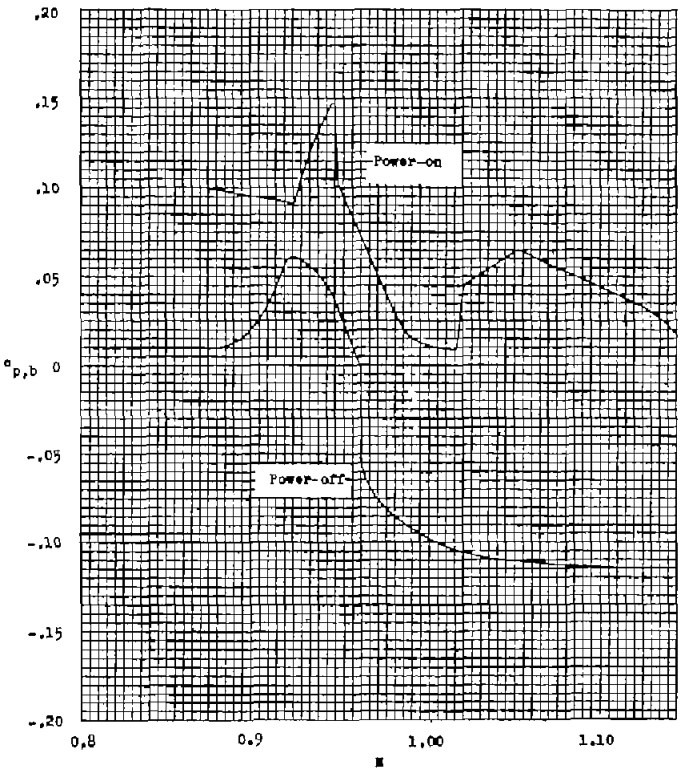

(j) Orifice J, model 2.

Figure 9.- Continued.

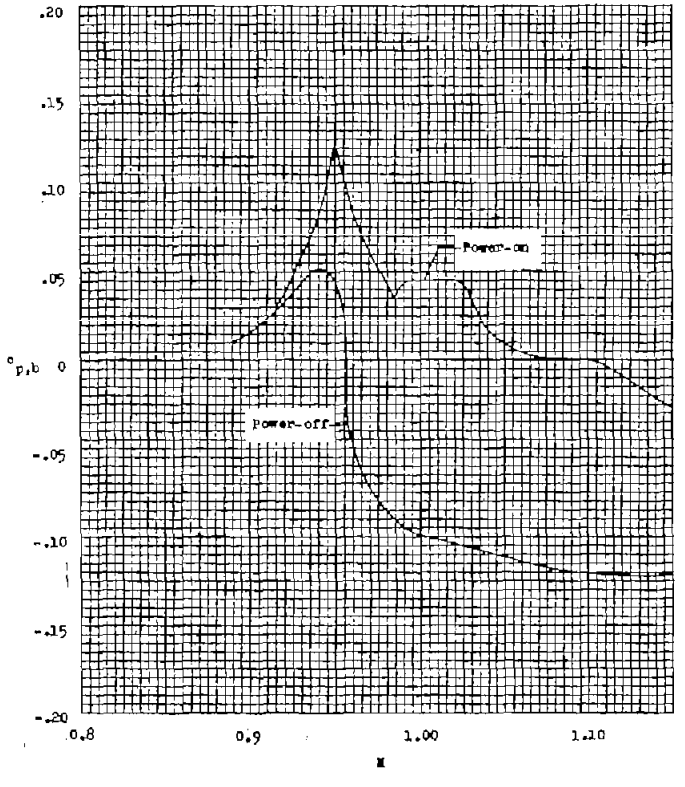

(k) Orifice K, model 2.

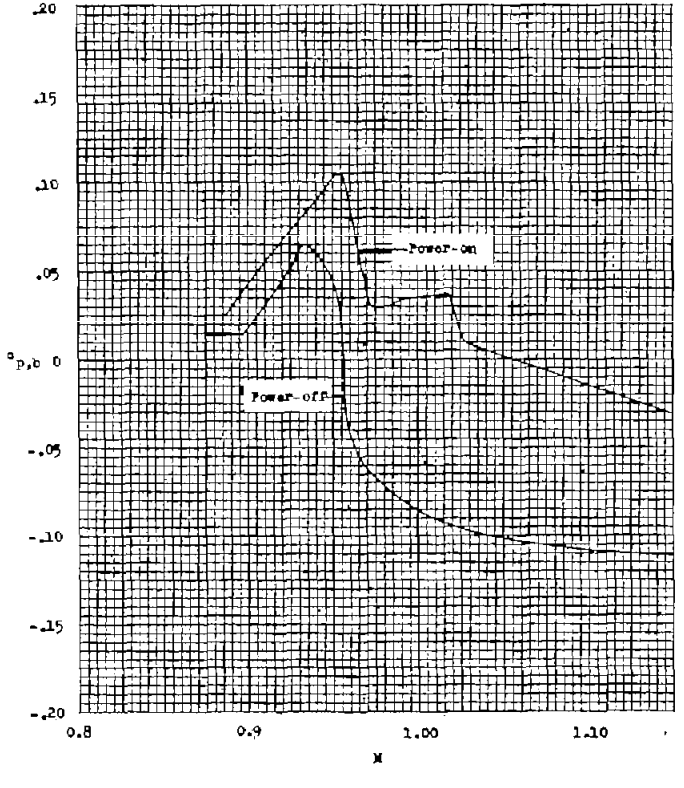

(l) Orifice L, model 2.

Figure 9.- Continued.

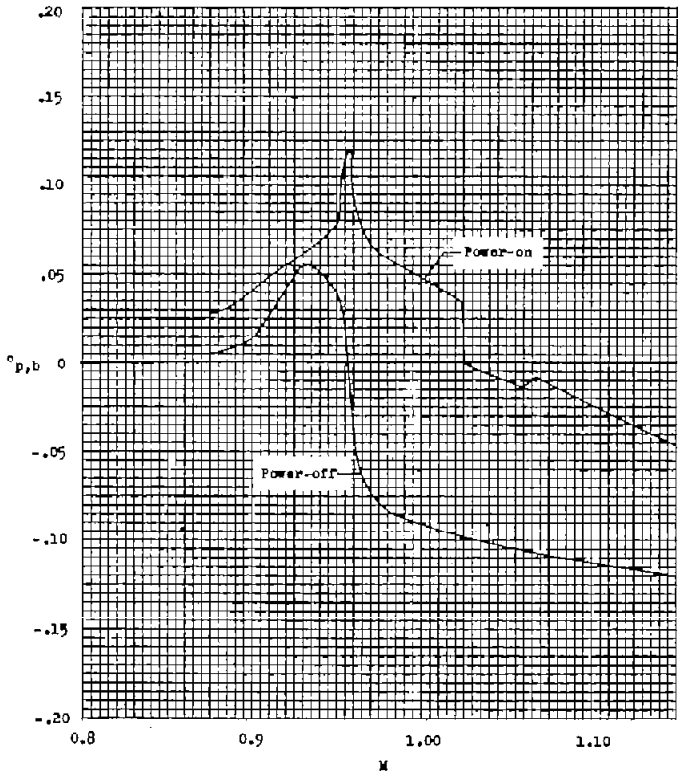

(m) Orifice M, model 2.

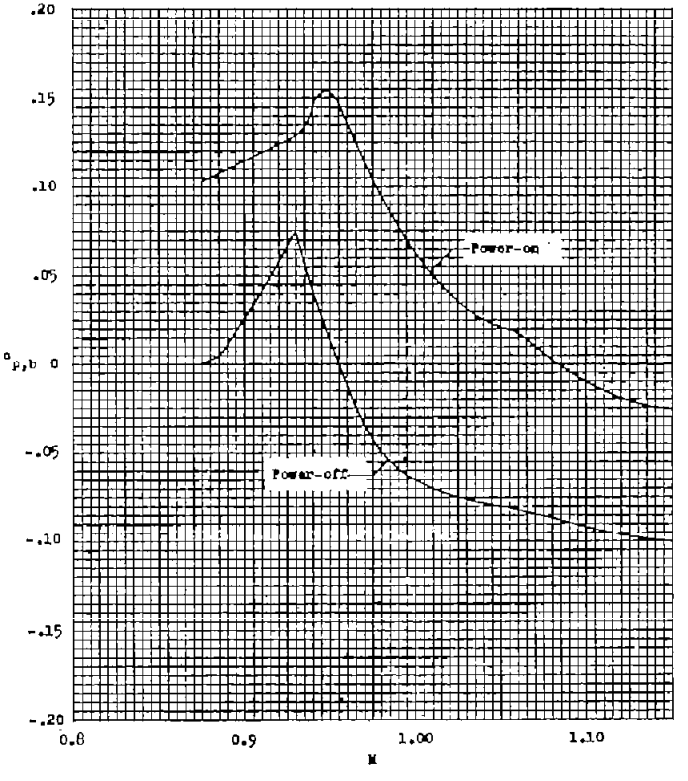

(n) Orifice N, model 2.

Figure 9.- Concluded.

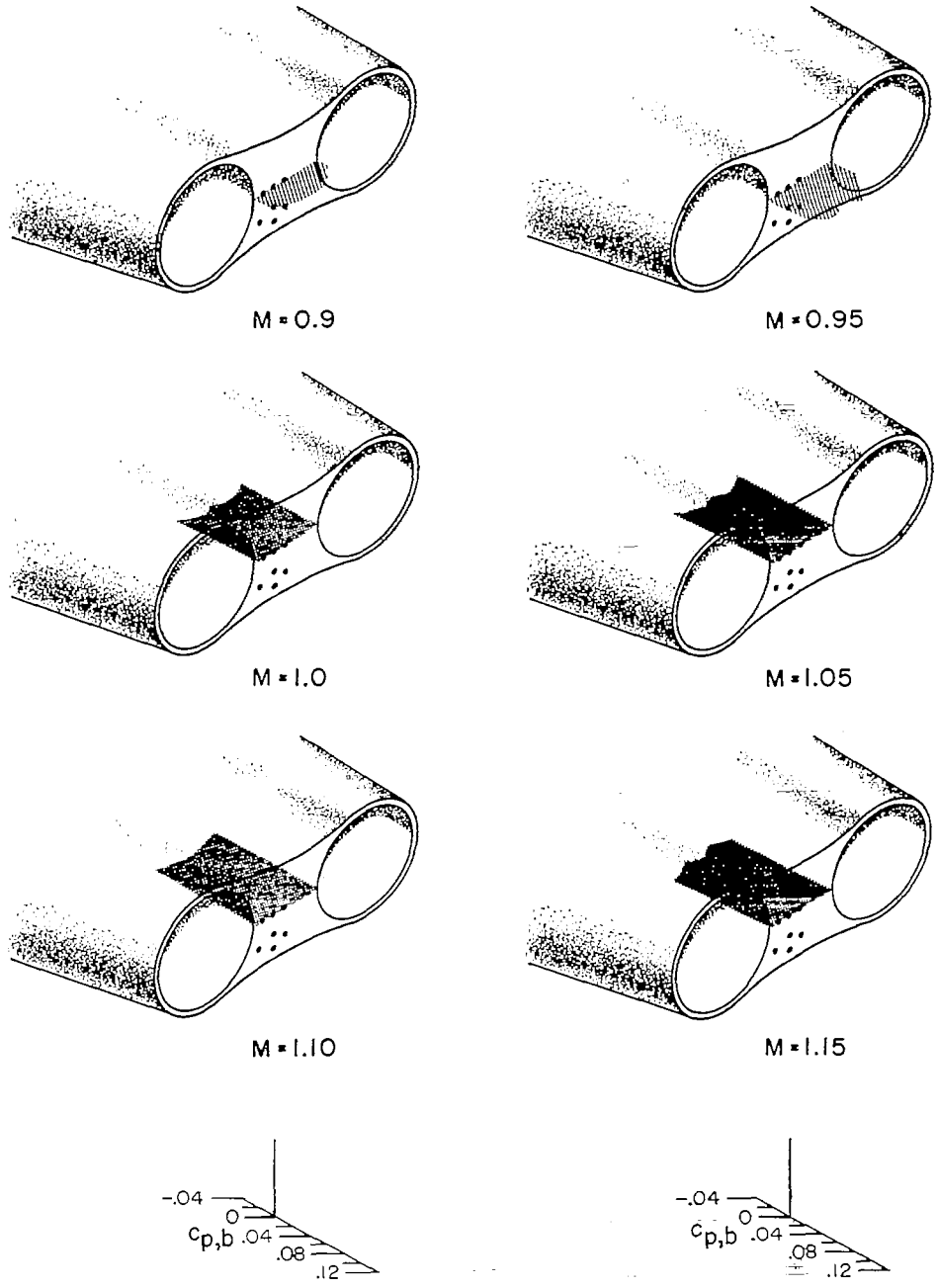

(a) Power off, model 1.

Figure 10.- Schematic diagram showing base-pressure variations for various free-stream Mach numbers along the horizontal axis of the base.

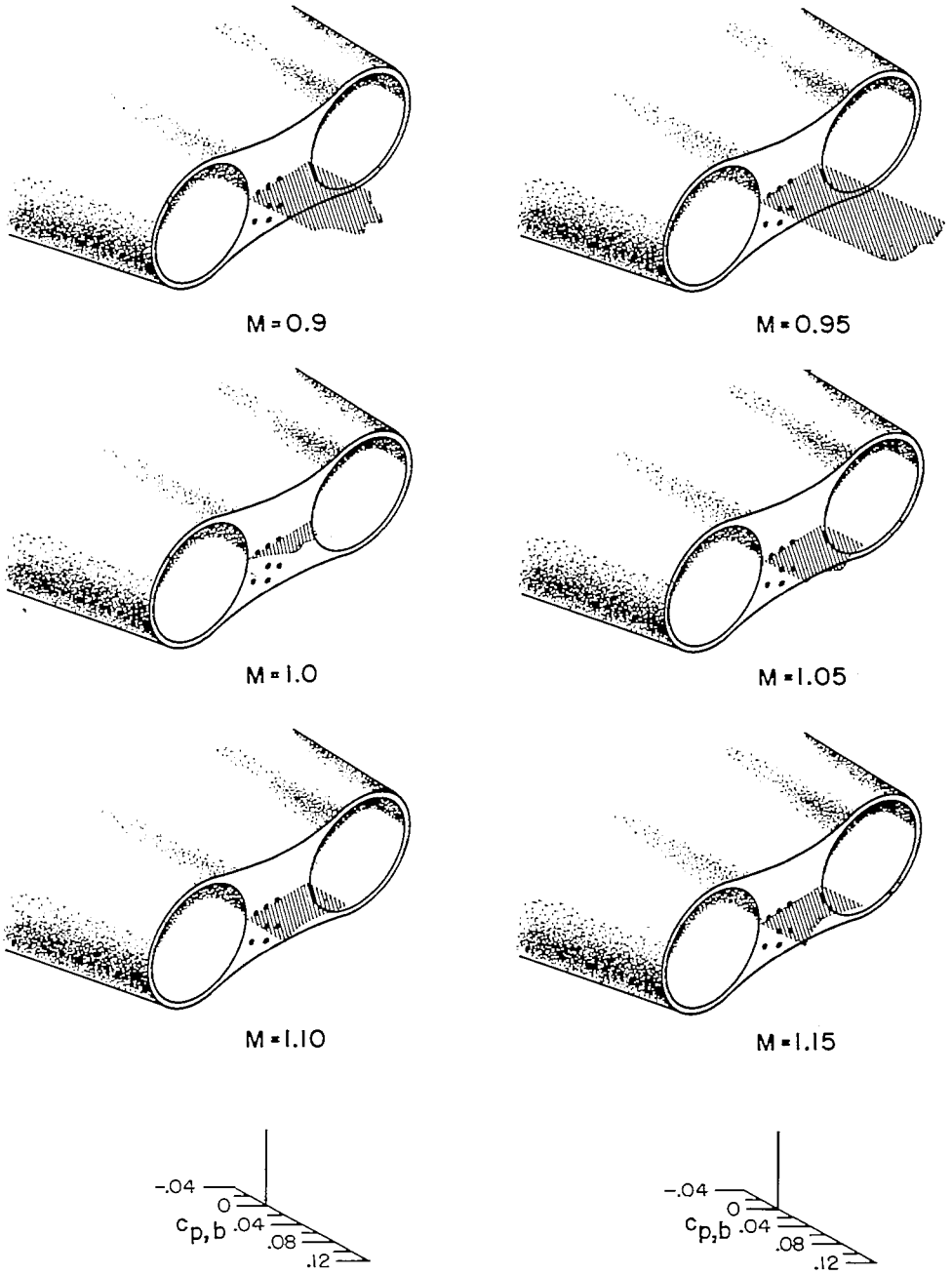

(b) Power on, model 1.

Figure 10.- Continued.

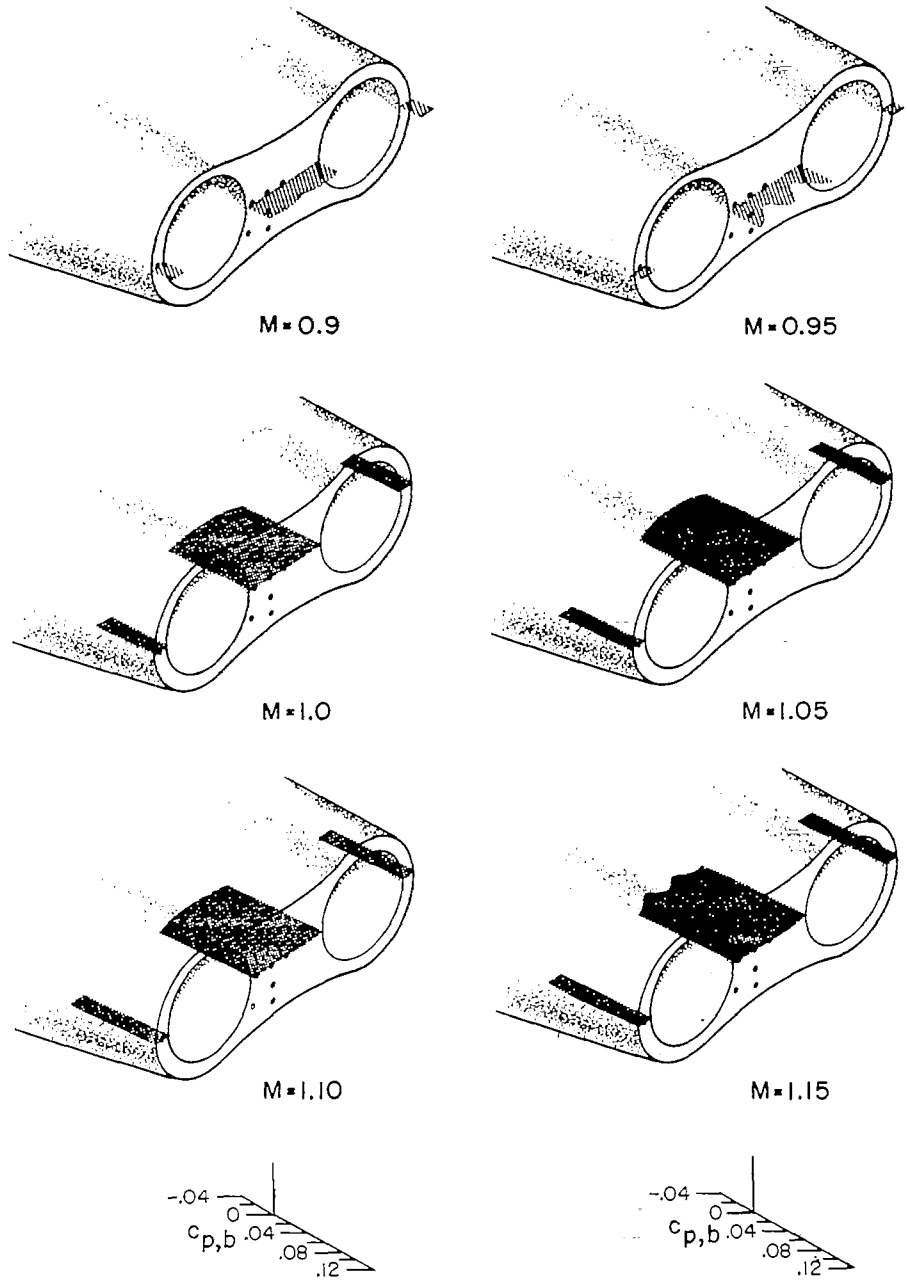

(c) Power off, model 2.

Figure 10.- Continued.

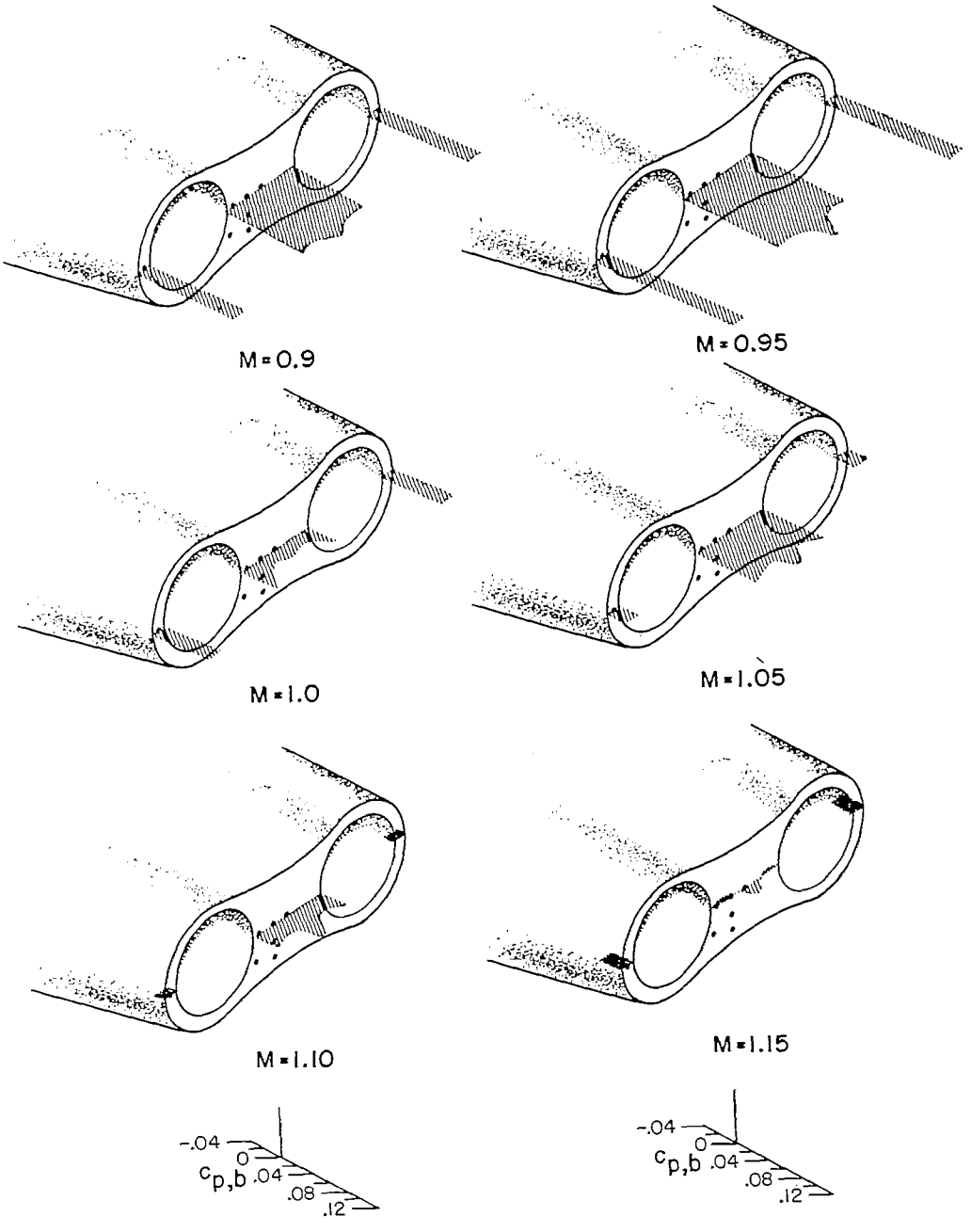

(d) Power on, model 2.

Figure 10.- Concluded.

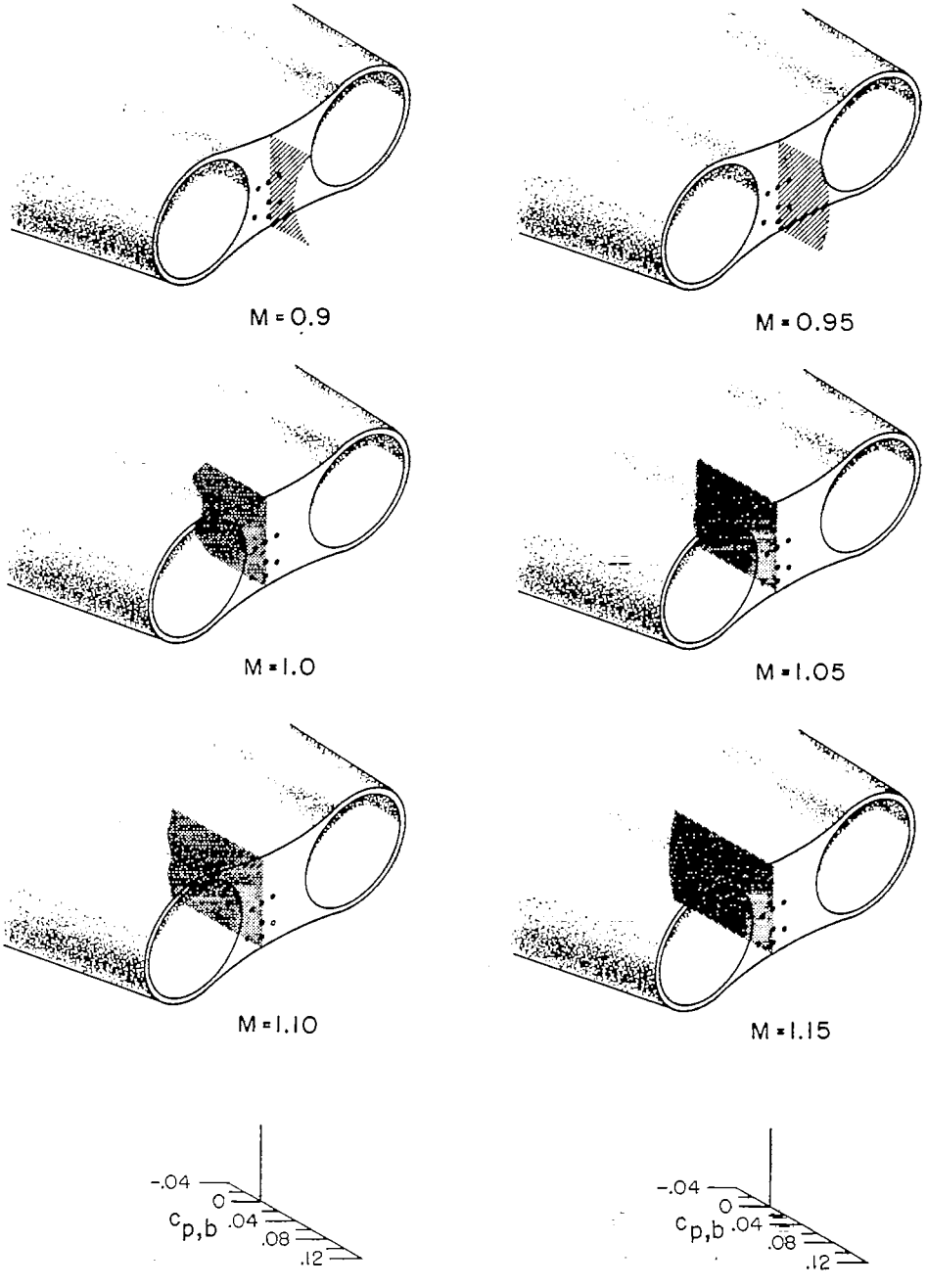

(a) Power off, model 1.

Figure 11.- Schematic diagram showing base-pressure variations for various free-stream Mach numbers along the vertical axis of the base.

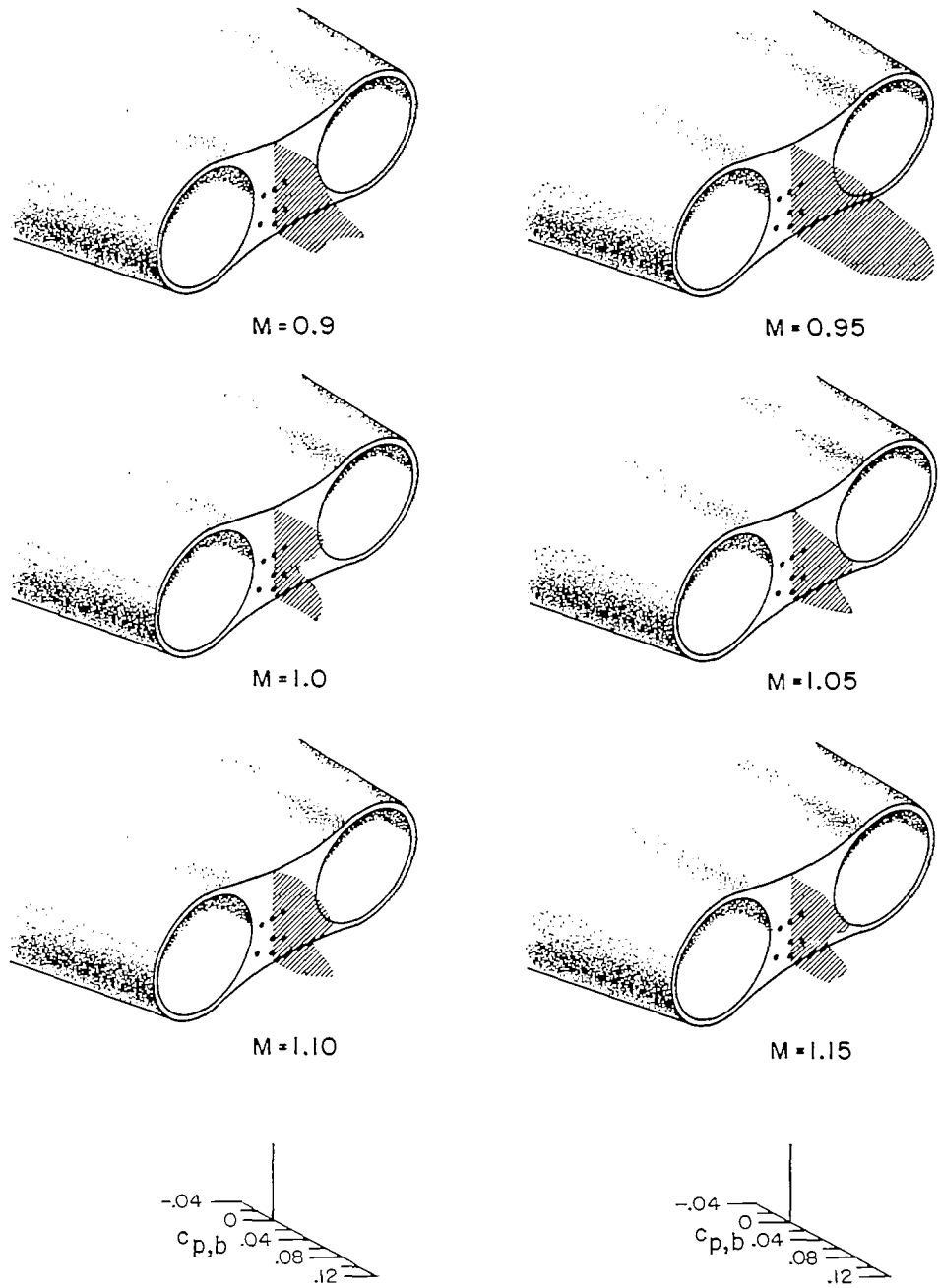

(b) Power on, model 1.

Figure 11.- Continued.

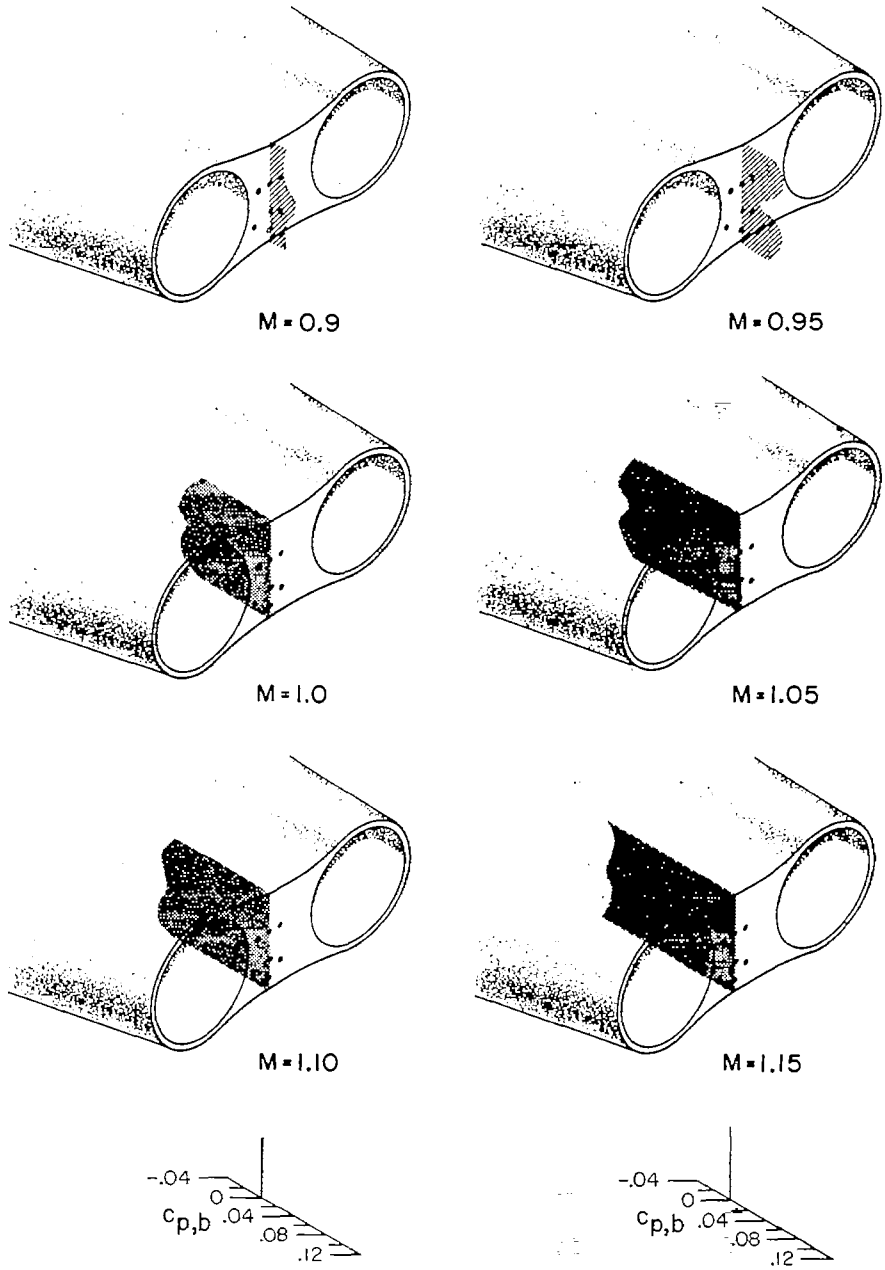

(c) Power off, model 2.

Figure 11.- Continued.

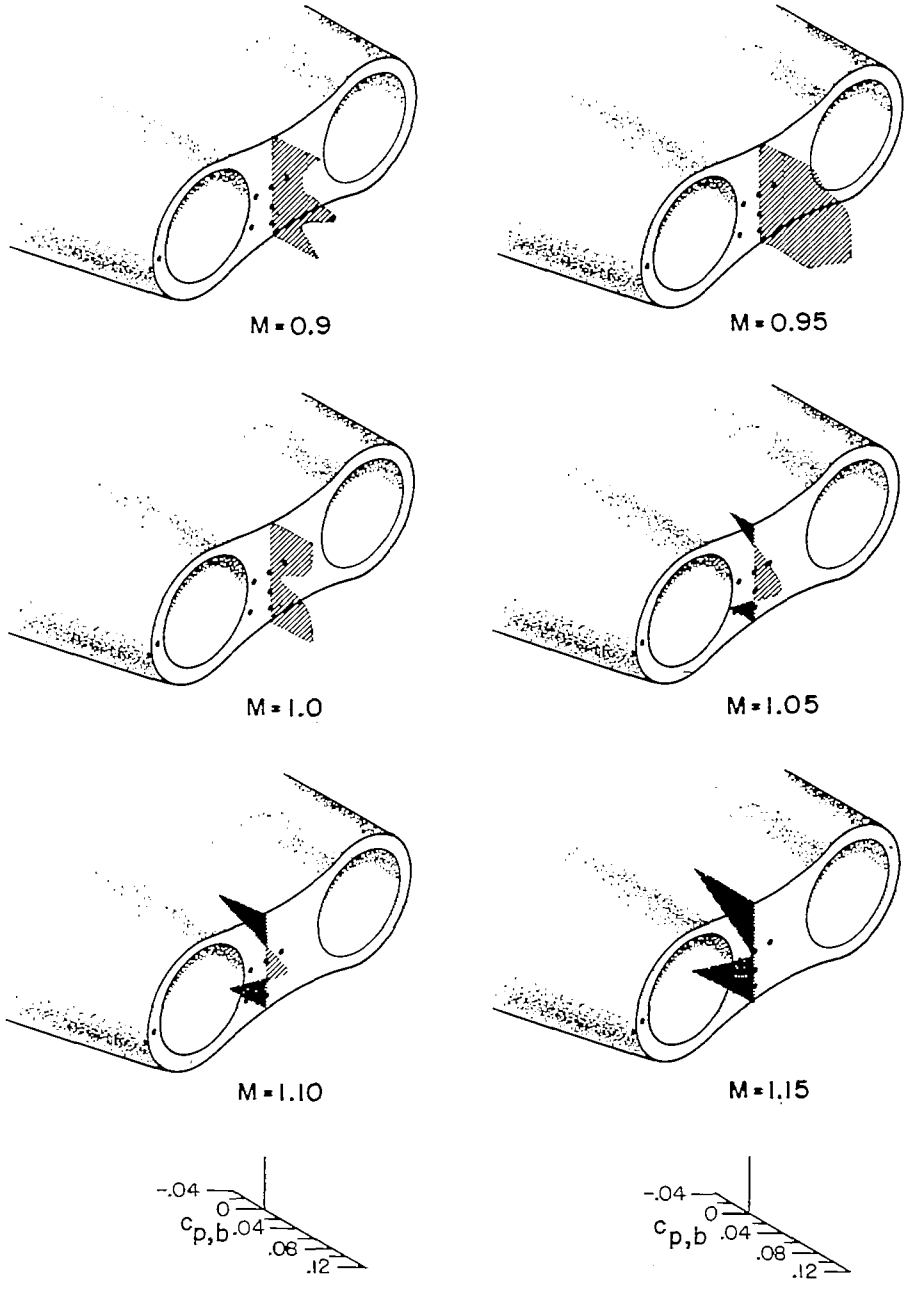

(d) Power on, model 2.

Figure 11.- Concluded.

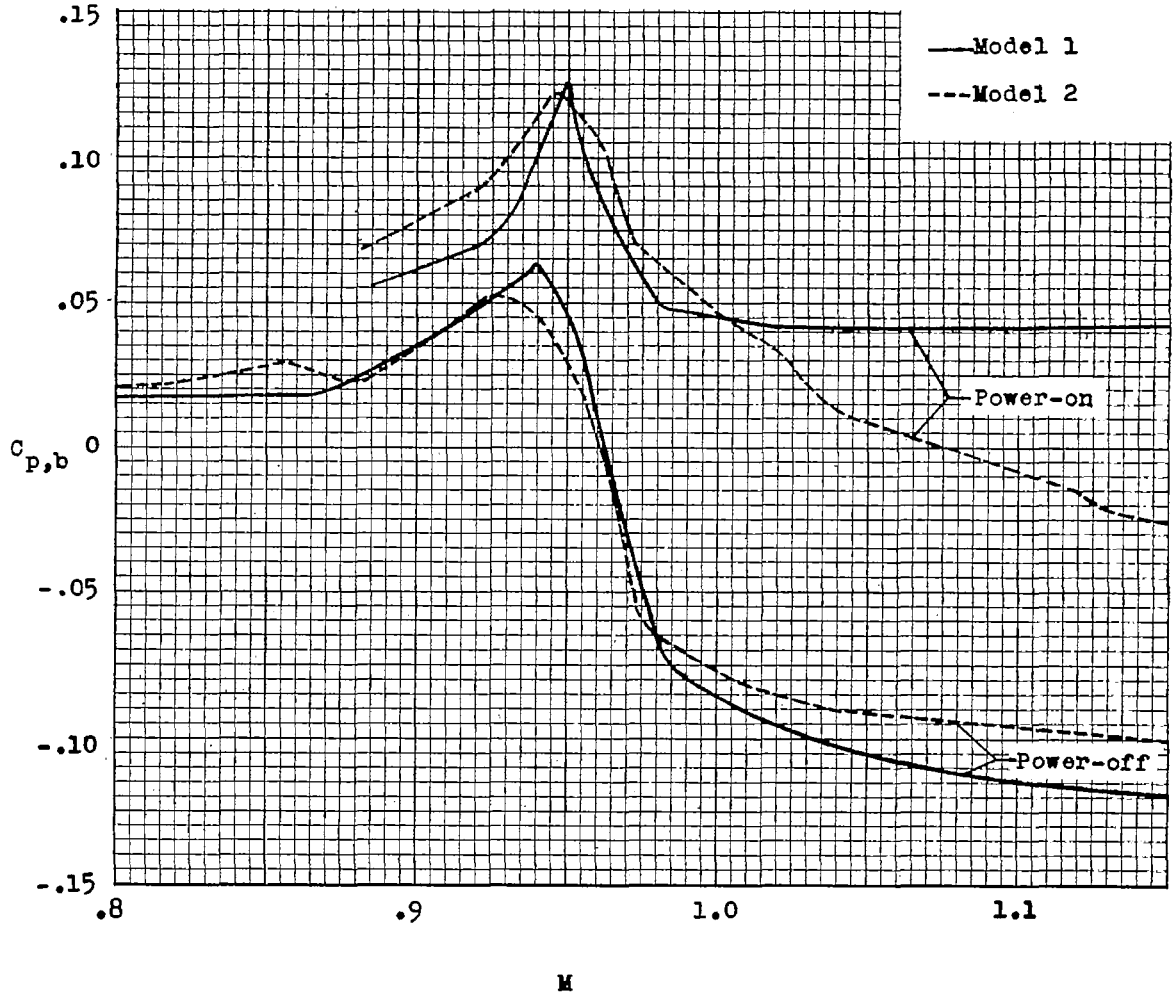

Figure 12.- Variation of average base pressure coefficients with Mach number for power-on and power-off conditions.

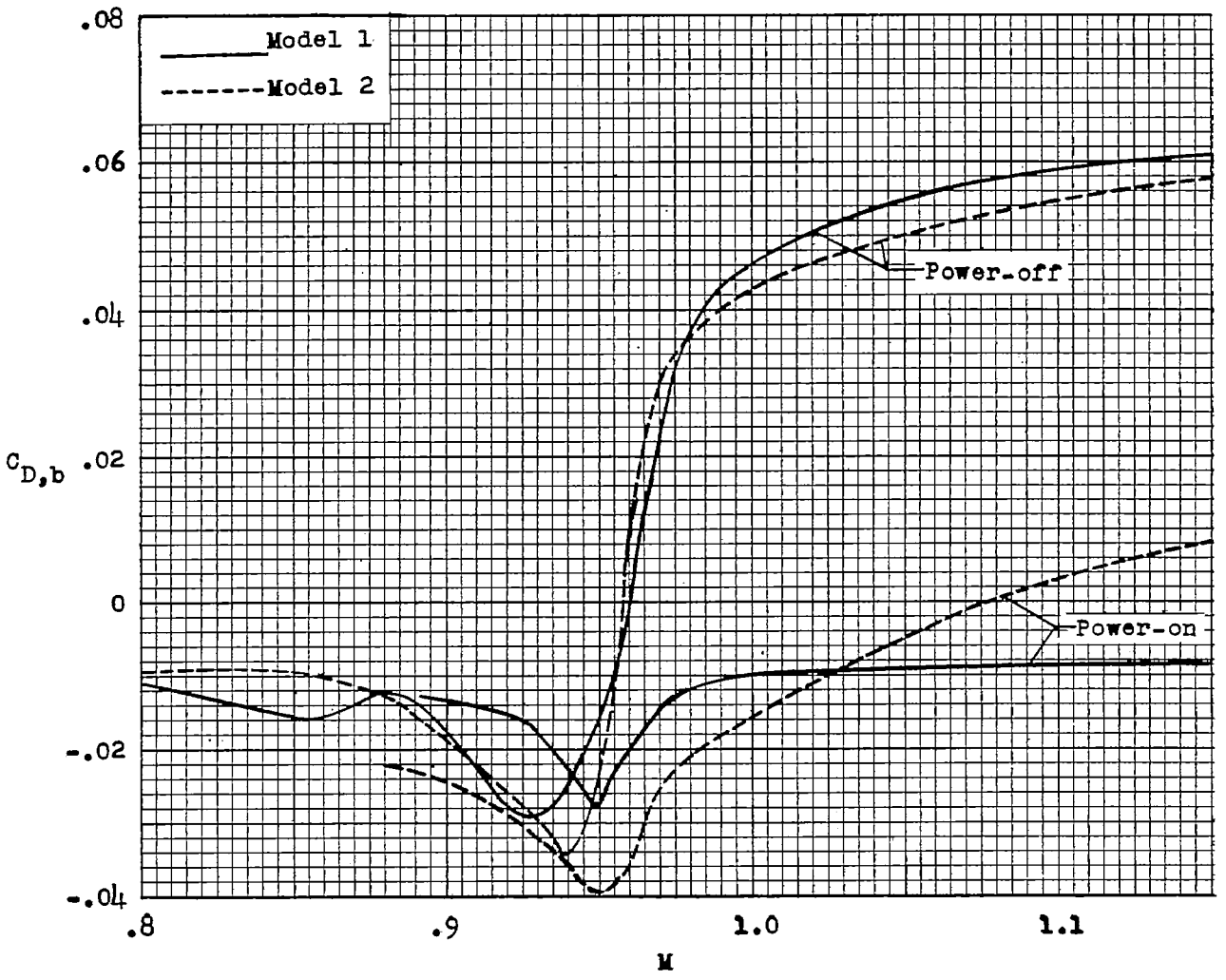

Figure 13.- Variation of total base drag coefficients with free-stream Mach number for power-on and power-off conditions.

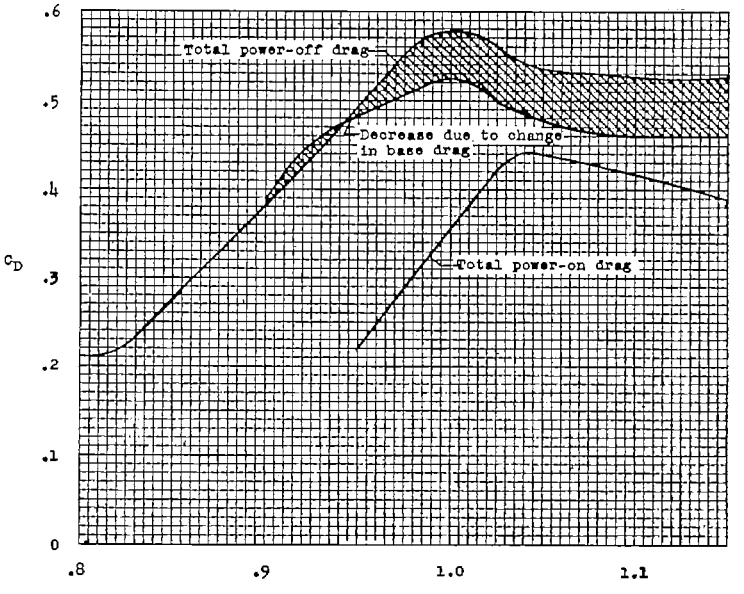

(a) Model 1.

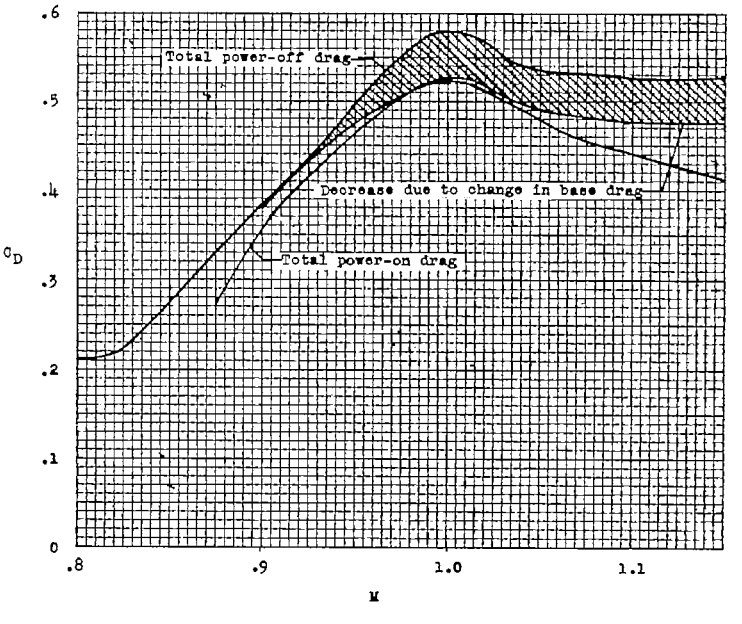

(b) Model 2.

Figure 14.- Variation of total drag with free-stream Mach number showing the amount of decrease in drag due to favorable power-on base drag.